Ecoepidemic predator-prey model with feeding satiation, prey herd behavior and abandoned infected prey

Kooi, B.W.; Venturino, E.

published in
Mathematical Biosciences
2016

DOI (link to publisher)
10.1016/j.mbs.2016.02.003

document version
Publisher's PDF, also known as Version of record

Mathematical Biosciences 274 (2016) 58–72

Contents lists available at ScienceDirect

Mathematical Biosciences

journal homepage: www.elsevier.com/locate/mbs

Ecoepidemic predator–prey model with feeding satiation, prey herd behavior and abandoned infected prey

Bob W. Kooi[a,*], Ezio Venturino[b]

[a] Faculty of Earth and Life Sciences, VU University, de Boelelaan 1085, 1081 HV Amsterdam, The Netherlands
[b] Dipartimento di Matematica "Giuseppe Peano", Università di Torino, via Carlo Alberto 10, 10123 Torino, Italy

ARTICLE INFO

Article history:
Received 2 October 2015
Revised 23 December 2015
Accepted 1 February 2016
Available online 10 February 2016

MSC:
37G35
92D30
92D25
92D40

Keywords:
Herd behavior
Disease transmission
Ecoepidemics
System collapse
Local and global bifurcations

ABSTRACT

In this paper we analyse a predator–prey model where the prey population shows group defense and the prey individuals are affected by a transmissible disease. The resulting model is of the Rosenzweig–MacArthur predator–prey type with an SI (susceptible-infected) disease in the prey. Modeling prey group defense leads to a square root dependence in the Holling type II functional for the predator–prey interaction term. The system dynamics is investigated using simulations, classical existence and asymptotic stability analysis and numerical bifurcation analysis. A number of bifurcations, such as transcritical and Hopf bifurcations which occur commonly in predator–prey systems will be found. Because of the square root interaction term there is non-uniqueness of the solution and a singularity where the prey population goes extinct in a finite time. This results in a collapse initiated by extinction of the healthy or susceptible prey and thereafter the other population(s). When also a positive attractor exists this leads to bistability similar to what is found in predator–prey models with a strong Allee effect. For the two-dimensional disease-free (i.e. the purely demographic) system the region in the parameter space where bistability occurs is marked by a global bifurcation. At this bifurcation a heteroclinic connection exists between saddle prey-only equilibrium points where a stable limit cycle together with its basin of attraction, are destructed. In a companion paper (Gimmelli et al., 2015) the same model was formulated and analysed in which the disease was not in the prey but in the predator. There we also observed this phenomenon. Here we extend its analysis using a phase portrait analysis. For the three-dimensional ecoepidemic predator–prey system where the prey is affected by the disease, also tangent bifurcations including a cusp bifurcation and a torus bifurcation of limit cycles occur. This leads to new complex dynamics. Continuation by varying one parameter of the emerging quasi-periodic dynamics from a torus bifurcation can lead to its destruction by a collision with a saddle-cycle. Under other conditions the quasi-periodic dynamics changes gradually in a trajectory that lands on a boundary point where the prey go extinct in finite time after which a total collapse of the three-dimensional system occurs.

1. Introduction

Recently the role of social behavior in the context of interacting populations has been introduced in predator–prey models. In the classical Rosenzweig–MacArthur model [19,20] both prey and predators have an homogeneous spatial distribution. The prey grows logistically in the absence of the predator and the natural predator mortality rate. The predator–prey interaction is described by a Holling type II functional response (the predation rate per predator which is a monotonic increasing prey-dependent hyperbolic relationship) where a handling time of the prey introduces feeding saturation. In [7] the predators are assumed to have a heterogeneous spatial distribution (for instance when they form a colony or school). Then the functional response depends on both predator and prey densities in a manner that reflects feeding interference between predators. This leads to a ratio-dependent or Beddington–DeAngelis type of functional response (see also [6]). In [10,21] on the other hand, the prey spatial distribution is heterogeneous giving group defense and the Holling type IV or Monod–Haldane functional response is used. This expression is also only prey-dependent but the function is now not monotonically increasing. The predation rate per predator decreases for larger prey densities. Bate and Hilker [4] note that Holling type IV functional responses usually result in an upper threshold of prey density, beyond which the predator cannot survive. Further, in recent work

* Corresponding author. Tel.: +31205987130; fax: +31295987123.
E-mail addresses: bob.kooi@vu.nl (B.W. Kooi), ezio.venturino@unito.it (E. Venturino).

http://dx.doi.org/10.1016/j.mbs.2016.02.003
0025-5564/

[11] the predators functional response is derived starting from first principles.

Here we study a different formulation with heterogeneous prey spatial distribution on the ground. The prey gather together in herds where only prey individuals that live close to the herds boundary on the ground are subject to hunting by predators. In [1,5,23,25] this feature has been taken into account in ecoepidemiological systems. These, besides ecological situations dealing with demographically interacting populations, consider also a transmissible disease in the system, see [16,24] for an introductory account.

In a parallel paper [8] an ecoepidemiological model in which the epidemics spread among the predators was proposed. Here we investigate a model where the prey are affected by a disease that propagates by contact. With respect to earlier formulations, these models exhibit the feature of feeding satiation, modeled via a Holling type II response function such as in the Rosenzweig–MacArthur model [20]. However, here the prey-dependent hyperbolic relationship is expressed as a function of the "square root" of the prey size instead of the prey size itself. It differs from the herd behavior model presented in [1], because it takes into account the feeding satiation phenomenon also explored in [8]. In the recent paper [4] a similar problem was studied but the predator group-defending prey functional response was the Holling type IV instead of the "square root" functional response.

The paper is organized as follows. In Section 2 we present the ecoepidemic model and the outline the methodology of the study. The two-dimensional models, the epidemic one, with infected prey population, and the purely demographic, i.e. disease-free, predator–prey model, are analysed respectively in Sections 3 and 4. Here we extend the analysis of [8] by a phase portrait analysis to study the total collapse of the system caused by a heteroclinic connection between the two prey-only saddle equilibria.

In Section 5 we move to the analysis of the full model where the prey is affected by the infectious disease, assuming that diseased individuals are left behind by the herd. We start with a classical existence and stability analysis of all equilibria in Sections 5.1 and 5.2. In Section 5.3, the numerical bifurcation analysis is carried out, completed for the special instance of codimension-two bifurcations. In addition to the bifurcations of the classical predator–prey models, i.e. transcritical, tangent (saddle node) and Hopf bifurcations, here also the torus (Neimark–Sacker) bifurcation occurs. A new phenomenon is represented by the abrupt destruction of the quasi-periodic dynamics on a torus similar to what was found in [3,6].

In Section 6 the results of all particular cases will be compared with the results of the ecoepidemic model with the infected predator population, instead of the prey, analysed in [8] and a final discussion concludes the paper. Assuming that the carrying capacity is sufficiently high to support coexistence of prey and predator, due to the weakening of the prey population by infection, the predator feeding on the prey population can persist for higher predators natural mortality rates.

2. Modeling and analysis approach

2.1. The model

We consider the model presented in [23], which we briefly illustrate again here for the convenience of the reader, to better emphasize the changes in that main model. The basic ecological model is an adapted Rosenzweig–MacArthur model first discussed in [19] where both prey and predators have an homogeneous spatial distribution. Mathematically, the consumption rate of the prey by the predator is expressed via a hyperbolic relationship.

In our case the spatial distribution of the prey population, forming a herd and occupying a certain portion of the ground, is heterogeneous. The prey individuals most subject to hunting are those close to the herd boundaries. The area occupied by the herd is proportional to the prey population and therefore to the size of the herd itself. The prey density on the herd perimeter is therefore proportional to the square root of the size of the herd and thus in the hyperbolic relationship of the standard Holling type II term, the prey size is here replaced by a square root of the prey size. The prey population grows logistically in the absence of the predator. In the absence of the prey, the predators die exponentially fast.

In order to model the spread of the disease, the prey population is divided into two classes consisting of healthy and diseased individuals. The latter are assumed to be too weak to reproduce and to compete for resources. Therefore the basic two-population demographic predator–prey model is extended into a three-dimensional predator—susceptible prey—infected prey model. As in the classical two compartmental SI-model the law of mass action is used to formulate the infection rate of the susceptible by infected prey, assuming possible contacts among all the individuals of the herd. The infected prey are assumed to be too weak both to reproduce and to compete for resources, i.e. they do not appear in the logistic reproduction function for the healthy prey. The infected prey are further assumed to drift away from the herd when become infected; this for instance occurs for elephants. But in the process, they are still able to infect other individuals in the herd. Once alone, they can easily be hunted by the predators. In view of the ease of these captures, we assume that the predators never get tired of hunting sick isolated prey individuals, this implying that in this case the hunting term is bilinear, i.e. a mass action term, as in the classical Lotka–Volterra model. On the other hand, as stated above, we assume that they can become satiated by hunting the healthy prey in the herd, observing that this hunt requires more effort than that one on the infected prey. Thus, mathematically, this is better modeled by a Holling type II response function. The predators' different attitudes in the prey capture therefore determine the different choices for the functional responses among healthy and infected prey.

The model where the state variables and parameters are overlined in order to be able to introduce re-scaled versions later, reads

$$\frac{d\overline{R}}{d\tau} = r\overline{R}\left(1-\frac{\overline{R}}{\overline{K}}\right) - \overline{\lambda}\,\overline{R}\,\overline{I} - \frac{\overline{a}\sqrt{\overline{R}}\,\overline{F}}{1+\overline{T}\,\overline{a}\sqrt{\overline{R}}}, \tag{1a}$$

$$\frac{d\overline{I}}{d\tau} = \overline{I}\left(\overline{\lambda}\,\overline{R} - \overline{b}\,\overline{F} - \overline{\mu}\right), \tag{1b}$$

$$\frac{d\overline{F}}{d\tau} = \overline{F}\left(\frac{\overline{e}\,\overline{a}\sqrt{\overline{R}}}{1+\overline{T}\,\overline{a}\sqrt{\overline{R}}} + \overline{e}\,\overline{b}\,\overline{I} - \overline{m}\right). \tag{1c}$$

The system consists of the equation for healthy prey $\overline{R}(\tau)$, reproducing logistically and being subject to the negative effects of hunting as well as to the infection process. The infected prey $\overline{I}(\tau)$ do not reproduce so that they are absent in the logistic growth term in the first equation, nor do they contribute to the population pressure on the susceptible prey, because we assume them to be too weak for that. The spread of the infection is modeled via a bilinear term with rate parameter $\overline{\lambda}$. The disease is unrecoverable, i.e. once entered into this class, an infected individual only exits it by dying at rate $\overline{\mu}$, incorporating natural plus disease-related effects or possibly by predation modeled with the Holling type I functional response with rate parameter $\overline{b}$. Note that here we disregard the possible healthy prey population pressure on the infected prey, i.e. we do not introduce a term of the type $\overline{c}\,\overline{R}\,\overline{I}$ into the second equation, assuming that the mortality is already represented by the linear term. Note also that the infected prey are assumed to be left behind by the herd, so that they are hunted on a one-to-one basis by the predators. Hence, they are also an "easy"

prey, not too difficult to capture because they are weakened by the disease, we assume that predators never get fed up with them and this explains the Holling type I functional response model formulation. Besides the infected prey, the predators gain from hunting healthy prey. This is expressed by a saturating Holling type II model containing the square root term for herd behavior. We thus distinguish hunting rates on healthy prey, indicated by $\overline{a}$ and on infected prey, expressed by the parameter $\overline{b}$. The conversion factor of both healthy and infected prey into new predators is the same $\overline{e}$.

As in the companion paper [8] we avoid the possible singularity appearing in the Jacobian matrix by letting $\overline{P} = \sqrt{\overline{R}}$. The non-dimensionalized model is obtained using the following substitutions

$$P(t) = \alpha\overline{P}(\tau), \quad F(t) = \beta\overline{F}(\tau), \quad I(t) = \gamma\overline{I}(\tau), \quad t = \delta\tau\ .$$

The system becomes

$$\frac{dP}{dt} = \frac{1}{2\delta}\left[rP\left(1-\frac{P^2}{\alpha^2\overline{K}}\right) - \frac{\overline{\lambda}}{\gamma}PI - \frac{\alpha^2}{\beta}\frac{\overline{a}}{\alpha+\overline{T}\,\overline{a}P}F\right],$$

$$\frac{dI}{dt} = \frac{I}{\delta}\left(\frac{\overline{\lambda}}{\alpha^2}P^2 - \frac{\overline{b}}{\beta}F - \overline{\mu}\right),$$

$$\frac{dF}{dt} = \frac{F}{\delta}\left(\frac{\overline{e}\,\overline{a}}{\alpha+\overline{T}\,\overline{a}P}P + \frac{\overline{e}\,\overline{b}}{\gamma}I - \overline{m}\right).$$

Let us define the following auxiliary parameters

$$\alpha = \overline{T}\,\overline{a}, \quad \delta = \frac{1}{2}\overline{r}, \quad \beta = \frac{\overline{\lambda}}{\overline{r}}, \quad \gamma = \overline{\lambda}\ .$$

where we now make the following choices:

$$\overline{r} = 2r, \quad \overline{K} = K, \quad \overline{\lambda} = \lambda, \quad \overline{\mu} = 2r\mu, \quad \overline{a} = a, \quad \overline{T} = T,$$
$$\overline{e} = e, \quad \overline{m} = m, \quad \overline{b} = \lambda b,$$

The final form of the system equations reads

$$\frac{dP}{dt} = P\left(1-\frac{P^2}{a^2KT^2}\right) - \frac{1}{\lambda}\frac{a^2T}{1+P}F - \frac{1}{2r}PI, \tag{2a}$$

$$\frac{dI}{dt} = 2I\left(\frac{\lambda}{2a^2rT^2}P^2 - bF - \mu\right), \tag{2b}$$

$$\frac{dF}{dt} = \frac{F}{r}\left(\frac{1}{T}\frac{e}{1+P}P + ebI - m\right). \tag{2c}$$

Our aim is to study the dynamics of the system depending on the prey carrying capacity K and the predator mortality rate m.

2.2. Methodology

The main mathematical analysis tool used is bifurcation theory whereby the dependency of the long-term dynamics on parameter variations is studied. We do this by calculation of the equilibria, limit cycles, quasi periodic solutions and chaos. To facilitate the numerical bifurcation analysis we have to choose parameter values. Unless stated otherwise, all the default parameter values used in our analysis are given in Table 1. We used the computer program AUTO [9] to perform the numerical bifurcation analysis of the equilibria and limit cycles.

During a process called continuation the dynamics is followed and changes in the long-term dynamics, for instance from stable to unstable equilibrium, are spotted. These points are called bifurcation points. Table 3 gives a list of the bifurcation points. Also the different line types of the bifurcations used in the diagrams are given. Further information about the basics of bifurcation analysis can be found in e.g. Guckenheimer and Holmes [12], Wiggins [26], Kuznetsov [15], and examples of ecological applications of bifurcation analysis in for instance [2] and [14,22] for the discussion of similar bifurcations as we will find here.

Table 1
List of symbols for variables and parameters and default parameter values used in the text. As the model does not concern a concrete ecosystem, the chosen parameter values are hypothetical. For those that have the same meaning as the model with the disease in the predators, we generally use the same values as in [8]. Note that the variable P is the square root of the prey population size.

Symbol	Value	Description
P	Variable	Healthy or susceptible prey
I	Variable	Diseased or infected prey
F	Variable	Predator
a	0.5	Hunting rate of predator on healthy prey
e	0.5	Conversion factor of prey into predators
K	Variable	Carrying capacity
m	Variable	Natural mortality rate of predators
r	0.7	Intrinsic growth rate of healthy prey
T	0.8	Average time to capture a healthy prey
t	Variable	Time
λ	0.7	Contact or infection rate for the prey disease
b	0.7	Contact rate of predator and diseased prey
μ	0.65	Natural+disease-related mortality of infected-prey

Table 2
List of the equilibrium points. In the figures, stable points are indicated by fill dots · and unstable points as empty dots ○. In one-parameter diagrams the stable equilibria and the maximum and minimum peak values of the limit cycles are solid curves and unstable versions are shown as dashed curves.

Attractor	Description
E_0	Zero-solution equilibrium
E_1	Disease-free prey-only equilibrium
E_{12}	Predator-free predator–prey equilibrium
E_{13}	Disease-free predator–prey equilibrium
L_{13}	Disease-free predator–prey limit cycle
E_{123}	Endemic predator–prey equilibrium
L_{123}	Endemic predator–prey limit cycle
T_{123}	Endemic predator–prey quasi-periodic torus dynamics

Table 3
List of the bifurcations points and curves. Also the different line types in the diagrams are given.

Bifurcation	Description
TC_1	Transcritical bifurcation (dashed curve) predator invasion into healthy prey P equilibrium E_1
TC_2	Transcritical bifurcation (dashed curve) infected prey invasion into prey equilibrium E_1
TC_3	Transcritical bifurcation (dashed curve) predator invasion into both prey PI equilibrium E_{12}
TC_4	Transcritical bifurcation (dashed curve) infected prey invasion into predator–prey PF equilibrium E_{13}
T	Tangent or saddle-node bifurcation (solid curve) collision of two equilibria or limit cycles
H_2	Hopf bifurcation for disease-free predator–prey system (dotted curve) origin of limit cycle
$H_3^{\pm}$	Hopf bifurcation for disease-free predator–prey system (dotted curve) origin of stable H^- or unstable H^+ limit cycle
TR	Torus bifurcation (long-dashed curve) destruction of limit cycle
B	Bautin bifurcation point change Hopf bifurcation for disease-free predator–prey system origin of tangent bifurcation of limit cycle
N	Codimension-two bifurcation point Intersection of codimension-one curves
$G^{\neq}$	Global bifurcation for disease-free predator–prey system (solid curve) Heteroclinic connection where destruction of limit cycle occurs Collapse of system and convergence to equilibrium E_0
S	Destruction of quasi-periodic solution on torus convergence to stable interior equilibrium E_{123}

The results are presented in bifurcation diagrams where bifurcation points or curves in the parameter space mark qualitative changes in the long-term dynamics (equilibria, limit cycles and quasi-periodic solutions). In bifurcation diagrams where the state variables are plotted as functions of time or of a parameter, solid (dashed) curves denote stable (unstable) equilibrium values. For limit cycle solutions they denote local maximum and minimum values. We used the computer program Maple [17] to do a symbolic analysis of equilibria. The classical ode45 ODE-solver of Matlab [18] was used to perform simulations by integration in time for specific parameter values and initial conditions.

Before we analyse the three-population system (2) , called the PIF-model, we start with the analysis of the two two-dimensional subsystems: the SI-model for the prey population, called the PI-model where $F = 0$ in (2), and then the demographic predator–prey model, called the PF-model where $I = 0$ in (2), with only healthy prey individuals.

3. The epidemic prey population model

Let us begin by studying the non-dimensionalized prey (healthy and diseased) only system *PI* where no predator is present. Strictly speaking the conversion from R to $P = \sqrt{R}$ is not necessary since the term with the square root in the predation term in (1a) and (2a) is missing. However, to be able to easily interpret the results obtained with those for the full PIF-model we adhere to model (2) with $F = 0$.

The dimensionless model where P represents healthy or susceptible prey and I is the diseased or infected prey population size reads

$$\frac{dP}{dt} = P\left(1 - \frac{P^2}{a^2KT^2}\right) - \frac{1}{2r}PI, \tag{3a}$$

$$\frac{dI}{dt} = 2I\left(\frac{\lambda}{2a^2rT^2}P^2 - \mu\right). \tag{3b}$$

In the next two sections we will study feasibility and stability of the equilibria of this *PI*-system (3).

3.1. *Equilibria:* PI-*system*

In the *PI* phase space, the equilibria $\widetilde{E}_k = (\widetilde{P}_k, \widetilde{I}_k)$ of the system (3) are found as follows. We have the origin $\widetilde{E}_0 = (0, 0)$, the disease-free $\widetilde{E}_1 = (aT\sqrt{K}, 0)$, and possibly the endemic prey population equilibrium $\widetilde{E}_{12} = (\widetilde{P}_2, \widetilde{I}_2)$, with

$$\widetilde{P}_2 = aT\sqrt{2\mu r}, \quad \widetilde{I}_2 = \frac{2r(\lambda K - 2\mu r)}{\lambda K}, \tag{4}$$

with feasibility condition

$$\lambda \geq \frac{2\mu r}{K}. \tag{5}$$

Observe that the carrying capacity K is involved in such a way that when the system is enriched (by increasing its carrying capacity K) the prey population becomes more vulnerable to the disease.

In Fig. 1 the vector field for $K = 20$ in combination with $m = 0.6$ is shown. The equilibrium E_{12} is the intersection of the two null-clines, the vertical curve is the I-null-cline where the time-derivative of I vanishes, i.e. the curve $P = aT\sqrt{2\mu r}$.

3.2. *Stability:* PI-*system*

The *PI* system (3) has the following Jacobian matrix

$$\widetilde{\mathbf{J}} = \begin{pmatrix} 1 - \dfrac{3P^2}{KT^2a^2} - \dfrac{I}{2r} & -\dfrac{P}{2r} \\ \dfrac{2\lambda IP}{ra^2T^2} & \dfrac{\lambda P^2}{ra^2T^2} - 2\mu \end{pmatrix}. \tag{6}$$

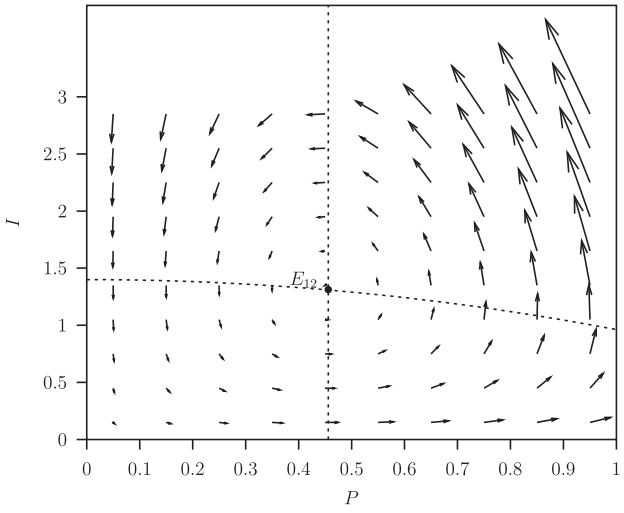

Fig. 1. Phase plane analysis of the PI-system (3) for the two state variables P and I, where $K = 20$ together with $m = 0.6$. There is a stable equilibrium E_{12} and the zero equilibrium E_0 is unstable. The interior equilibrium E_{12} is the intersection of the two null-clines (dashed lines).

At the origin the eigenvalues of the Jacobian matrix are $\widetilde{\omega}_{01} = 1$, $\widetilde{\omega}_{02} = -2\mu$, showing that $\widetilde{E}_0$ is always an unstable equilibrium. Their respective eigenvectors are $(1, 0)^T$ (unstable manifold) and $(0, 1)^T$ (stable manifold). This will be an important fact when we study the full three-dimensional model below.

At equilibrium $\widetilde{E}_1$ where $P = aT\sqrt{K} > 0, I = 0$ we find the following Jacobian matrix $\widetilde{\mathbf{J}}_1 = \widetilde{\mathbf{J}}(\widetilde{E}_1)$

$$\widetilde{\mathbf{J}}_1 = \begin{pmatrix} -2 & -\dfrac{aT\sqrt{K}}{2r} \\ 0 & \dfrac{\lambda K}{r} - 2\mu \end{pmatrix}. \tag{7}$$

The eigenvalues of the Jacobian matrix at $\widetilde{E}_1 = (aT\sqrt{K}, 0)$ read $\widetilde{\omega}_{11} = -2$ and $\widetilde{\omega}_{12} = (\lambda K - 2r\mu)/r$. Thus equilibrium $\widetilde{E}_1$ is stable for

$$K < \frac{2r\mu}{\lambda} \stackrel{\text{def}}{=} \widetilde{K}^{\dagger} \tag{8}$$

and unstable conversely. The parameter value $K^{\dagger} = 1.3$ for the default parameter values, marks a so called transcritical bifurcation parameter TC_{12} in general identified by the criterion $\det \mathbf{J}_1 = \mathbf{J}(\widetilde{E}_1) = 0$. Invasion of the disease is possible when the boundary, disease-free equilibrium $\widetilde{E}_1$ becomes unstable. To which kind of interior long-term dynamics (whether be it an equilibrium, a limit cycle or chaotic attractor) this invasion leads to is, however, not predicted. On the other hand we know that there is an interior equilibrium given in (4) when the feasibility condition (5) is fulfilled.

The eigenvalues of the Jacobian matrix evaluated at the endemic equilibrium $\widetilde{E}_{12}$ are explicitly evaluated as

$$\widetilde{\omega}_{21} = 2\frac{-r\mu + \sqrt{r^2\mu^2 - (\lambda K - 2r\mu)\mu\lambda K}}{\lambda K},$$

$$\widetilde{\omega}_{22} = 2\frac{-r\mu - \sqrt{r^2\mu^2 - (\lambda K - 2r\mu)\mu\lambda K}}{\lambda K}.$$

The expression in the square root term is always smaller than $r^2\mu^2$, in view of the feasibility condition (5). Hence, when the discriminant is positive both eigenvalues are real and negative and the equilibrium is a stable node. On the other hand when the discriminant is negative the real part of the conjugate eigenvalues is negative and the equilibrium is a stable focus. Hence, stability of the equilibrium $\widetilde{E}_{12}$ given by (4) of the endemic prey system is ensured when condition (5) is satisfied.

There is no Hopf bifurcation since the real part of the conjugate eigenvalues differs from zero. In general the Hopf bifurcation of a two-dimensional system occurs when $\mathrm{tr}\mathbf{J}_{12} = 0$, that is the trace of the Jacobian matrix is zero. Here we have $\mathbf{J}_{12} = \widetilde{\omega}_{21} + \widetilde{\omega}_{22} = -4r\mu/(\lambda K) \neq 0$.

4. The demographic predator–prey model

We begin by recalling and extending some interesting results already obtained in [5,8] for the disease-free or purely demographic model *PF*. Here we give the extended model formulation, assess its the equilibria and their stability. But furthermore and most importantly for the following analysis of this paper, we perform the full bifurcation analysis and state its results.

In non-dimensionalized form, the model derived in [8], reads as follows, where P denotes prey population size and F again denotes the predator size:

$$\frac{dP}{dt} = P\left(1 - \frac{P^2}{a^2T^2K}\right) - \frac{1}{\lambda}\frac{a^2T}{1+P}F, \tag{9a}$$

$$\frac{dF}{dt} = \frac{F}{r}\left(\frac{1}{T}\frac{e}{1+P}P - m\right). \tag{9b}$$

This model is obtained by taking $I = 0$ in (2).

In the next sections we perform an existence and stability analysis of the equilibria of this *PF*-system (9) completed by a bifurcation analysis where we also study the existence and stability analysis of limit cycles.

4.1. *Equilibria:* PF-*system*

In the *PF* phase space the equilibria $\widehat{E}_k = (\widehat{P}_k, \widehat{F}_k)$ of the system (9) are: the origin $\widehat{E}_0 = (0,0)$, the predator-free point $\widehat{E}_1 = (aT\sqrt{K}, 0)$, and possibly coexistence $\widehat{E}_{13} = (\widehat{P}_3, \widehat{F}_3)$, with

$$\widehat{P}_3 = \frac{mT}{e - mT}, \quad \widehat{F}_3 = m\lambda e\frac{a^2K(e-mT)^2 - m^2}{a^4K(e-mT)^4}. \tag{10}$$

It is feasible for $0 \leq \widehat{P}_3 \leq aT\sqrt{K}$, i.e. explicitly for

$$e \geq mT, \quad m \leq \frac{ae\sqrt{K}}{1 + aT\sqrt{K}} \stackrel{\text{def}}{=} \widehat{m}^{\dagger}. \tag{11}$$

4.2. *Stability:* PF-*system*

The *PF* system (9) has the following Jacobian matrix

$$\widehat{\mathbf{J}} = \begin{pmatrix} 1 - \dfrac{3P^2}{KT^2a^2} + \dfrac{a^2TF}{\lambda(1+P^2)} & -\dfrac{a^2T}{\lambda(1+P)} \\ \dfrac{eF}{rT(1+P)} - \dfrac{eFP}{rT(1+P)^2} & \dfrac{eP}{rT(1+P)} - \dfrac{m}{r} \end{pmatrix}. \tag{12}$$

The eigenvalues of the Jacobian matrix of (9) evaluated at the origin are $\widehat{\omega}_{01} = 1$, $\widehat{\omega}_{02} = -m/r$; their respective eigenvectors are $(1, 0)^T$ and $(1, \lambda(r+m)(ra^2T)^{-1})^T$. Thus $\widehat{E}_0$ is an unstable saddle.

At equilibrium $\widehat{E}_1$ the eigenvalues of $\widehat{\mathbf{J}}_1$ read

$$\widehat{\omega}_{11} = -2, \quad \widehat{\omega}_{12} = -\frac{1}{r}\left(\frac{ea\sqrt{K}}{1 + aT\sqrt{K}} - m\right).$$

Thus equilibrium $\widehat{E}_1$ is stable for $\widehat{m}^{\dagger} > m$ and unstable conversely, (see (11)). The parameter value $m\dagger$ marks a so called transcritical bifurcation parameter TC_1. Invasion of the prey is possible when the boundary equilibrium $\widehat{E}_1$ becomes unstable. To which kind of interior long-term dynamics (equilibrium, limit cycle or chaotic attractor) this invasion leads to is not predictable from this information.

There is an interior equilibrium $\widehat{E}_{13}$, see (10), when the feasibility condition (11) is fulfilled.

The matrix $\widehat{\mathbf{J}}$ of the *PF*-system given in (12) is now evaluated for $P = \widehat{P}_3$ and $F = \widehat{F}_3$ given in (10). The eigenvalues are

$$\omega_{21,22} = \frac{1}{2}\left(\mathrm{tr}(\widehat{\mathbf{J}}) \pm \sqrt{\mathrm{tr}(\widehat{\mathbf{J}})^2 - 4\det(\widehat{\mathbf{J}})}\right).$$

with

$$\mathrm{tr}(\widehat{\mathbf{J}}) = r\left(1 - \frac{3\widehat{P}_3^2}{a^2K}\right) + \frac{a^2K}{T}\frac{1}{(1+\widehat{P}_3)^2}\widehat{F}_3, \tag{13}$$

$$\det(\widehat{\mathbf{J}}) = \frac{2e}{T^2}\frac{a^2K}{(1+\widehat{P}_3)^3}\widehat{F}_3. \tag{14}$$

The interior equilibrium $\widehat{E}_{13}$ is stable when $\mathrm{tr}(\widehat{\mathbf{J}}) < 0$.

The region in the parameter space (K, m) where the interior equilibrium $\widehat{E}_{13}$ is stable is bounded by the codimension-one transcritical TC_1 and Hopf H_2 bifurcation curves. The codimension-one transcritical bifurcation curve TC_1 specified by $\det\widehat{\mathbf{J}}_{13} = 0$ is described by

$$K_{TC_1} = \left(\frac{m}{a(e-mT)}\right)^2. \tag{15}$$

It has a horizontal asymptote for $m = e/T = 0.625$ for the default parameter values given in Table 1. The Hopf bifurcation curve for this two-dimensional system is given by the trace $\mathrm{tr}\mathbf{J}_{13} = 0$

$$K_{H_2} = \frac{m^2(mT+3e)}{a^2(m^3T^3 - em^2T^2 - me^2T + e^3)}. \tag{16}$$

In the next subsection these bifurcation curves are calculated using the program AUTO [9] for the specific parameter set given in Table 1.

4.3. *Bifurcation analysis:* PF-*system*

In order to study equilibrium E_{13} and the limit cycle L_{13} originating at the Hopf bifurcation, we use a numerical bifurcation analysis where K and m are taken as the variable parameters while all other ones are fixed at the default values given in Table 1.

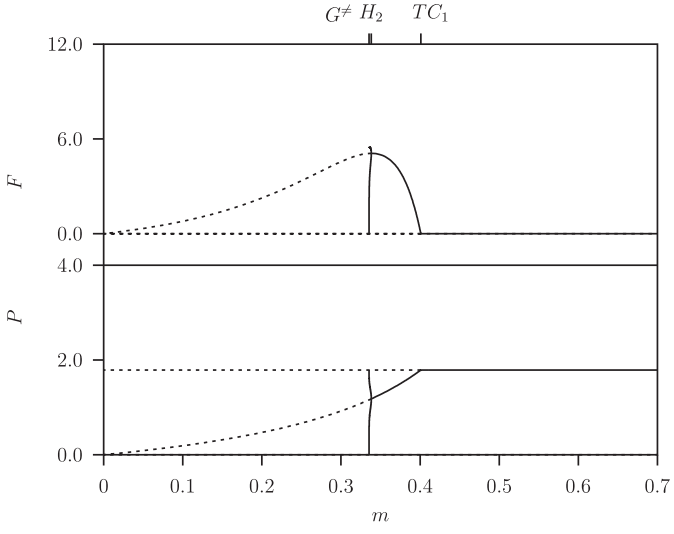

Fig. 2. One-parameter bifurcation diagram for $K = 20$ and free parameter m, for the demographic *PF* system (9) for the healthy prey population, P and the predator population, F. The solid curve between the transcritical bifurcation point TC_1 and the Hopf bifurcation point H_2 denotes stable equilibrium E_{13} values. Below H_2 the equilibrium E_{13} is unstable and shown as a dashed curve. Between H_2 and the global bifurcation point $G^{\neq}$ the maximum and minimum peak values of the stable limit cycle L_{13} are shown as solid curves. Table 2 gives a list of the asymptotic dynamics and Table 3 gives a list of the bifurcations.

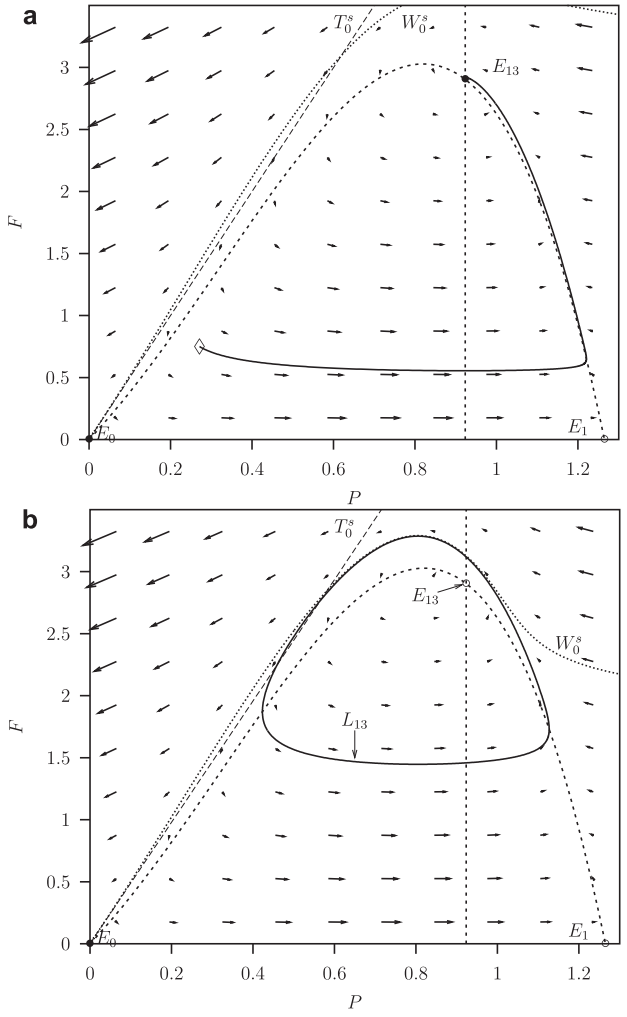

Fig. 3. Phase plane analysis of the demographic system (9) for the two state variables $P \geq 0$ and F predator population, where $K = 10$. (a) Where $m = 0.3$ and starting from initial point labeled by a '◇' with trajectory (solid curve) converging to the stable equilibrium E_{13} that is the intersection of the two null-clines (dashed lines). (b) Where $m = 0.278745$ with convergence to the stable limit cycle L_{13} (solid curve). The straight curve (long-dashed curve) is the linear tangent manifold T_0^s which is tangent to and is a local approximation of stable manifold W_0^s (dotted curve).

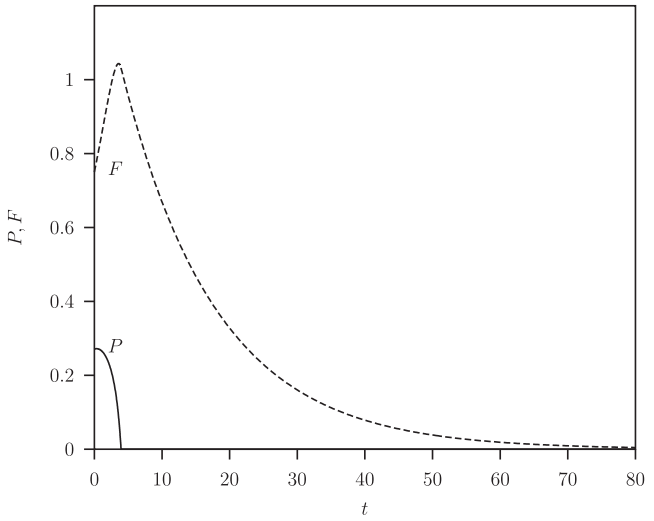

Fig. 4. Solution of the demographic system (9) for the two state variables, the prey $P \geq 0$ (solid curve), and the predator population F (long-dashed curve), as function of time t, where $K = 1$ and $m = 0.05$. In the corresponding phase plane plot of Fig. 5 this trajectory is shown as the solid line starting from the point labeled by a '◇'. The unstable interior equilibrium E_{13} is the intersection of the two null-clines (dashed lines).

The one-parameter bifurcation diagram is shown in Fig. 2 where m is the bifurcation parameter and $K = 20$. With large mortality rates (say $m = 0.7$) only the prey population persists. Decreasing the parameter m the predator population invades at the transcritical bifurcation TC_1 leading to the existence of the interior solution of the predator–prey PF system (9). Decreasing the mortality m further the predator population size increases and at the Hopf bifurcation, H_2, a limit cycle L_{13} occurs. Lowering m the amplitude of these limit cycles grows fast. It is broken by a heteroclinic connection between two saddle equilibrium points where $F = 0$ at the global bifurcation point $G^{\neq}$ at $m = 0.335475$, (see also [8,22]). Related to this phenomenon is the fact that equilibrium E_0 is reached in a finite time as it will be shown below.

The pictures in Fig. 3 show the vector field for $K = 10$ in combination with $m = 0.3$ and 0.278745 respectively. The trajectories shown terminate asymptotically in the stable equilibrium E_{13} and stable limit cycle L_{13}, respectively. From the origin three curves originate. The dotted line is a numerical approximation of the stable manifold W_0^s passing through E_0 calculated by time backbackward simulations. The long-dashed curve is the linear tangent manifold T_0^s passing through E_0 which is a local approximation of the tangent to the stable manifold W_0^s corresponding to the negative eigenvalue $-m/r$ with eigenvector $(1, (r+m)\lambda(a^2Tr)^{-1})^T$.

The vector fields in Fig. 3 reveal that for points starting above the curve W_0^s leads to crossing the vertical axis where $P = 0$. In order to explain this fact, we revisit the dynamics analysis. The Jacobian matrix evaluated at the origin E_0 yields the eigenvalues 1 and $-m/r$ and the eigenvectors $(1, 0)^T$ and $(1, (r+m)\lambda(a^2Tr)^{-1})^T$. This means that for the dynamics restricted to the line $P = 0$ the single eigenvalue is negative $-m/r$ and that equilibrium E_0 is stable once $P(t)$ vanishes in finite time. There can be bistability when there is an interior limit set, for instance the stable equilibrium E_{13} or the stable limit cycle L_{13}. In order to substantiate this statement we simulated backward in time the system starting from points where $P(0) = 0$ and $F(0) > 0$ but close to zero. These calculated trajectories are the dotted lines in Fig. 3. They form approximately the stable manifolds W_0^s passing through E_0 which act as separatrix between E_0 and E_{13} or L_{13}. In each figure the linear tangent manifold T_0^s is the straight long-dashed curve passing through E_0 which is tangent to and is a local approximation of stable manifold W_0^s corresponding to the negative eigenvalue $-m/r$ with eigenvector $(1, (r+m)\lambda(a^2Tr)^{-1})^T$.

In Fig. 4 the population solutions for the parameter combinations $K = 1$ and $m = 0.05$ are shown where the zero equilibrium is globally attracting, that is there is no stable equilibrium E_{13} nor stable limit cycle L_{13}. These results show that the prey population P goes extinct in finite time. The time of extinction depends on the initial conditions. Thereafter the predator population F goes extinct asymptotically, despite the fact that the origin equilibrium E_0 was unstable. This is a result of the non-uniqueness of the solution due to the square root singularity of the ODE that describes the dynamics of the prey population P.

The vector field close to the origin is shown in Fig. 5. The dashed curves are the null-clines, the vertical curve is the F-null-cline where the time-derivative of F vanishes, i.e. the curve $P = mT(e - mT)^{-1}$. This curve goes through the unstable internal equilibrium E_{13} where it intersects the P-null-cline where the time-derivative of P vanishes. The P-null-cline intersects the horizontal curve at the origin $\widehat{E}_0$ and at $\widehat{E}_1$ where $P = aT\sqrt{K} = 0.4$ and $F = 0$. Note that the arrows cross the vertical axis, the line $P = 0$, with rate $dP/dt = -(a^2T/\lambda)\,F$ and it is negative for $F > 0$. The solid line

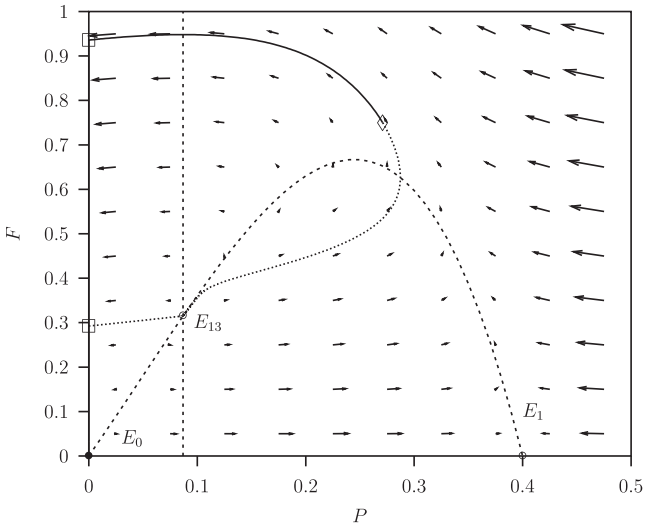

Fig. 5. Phase plane analysis of the demographic system (9) for the two state variables $P \geq 0$ and F predator population, where $K = 1$ and $m = 0.05$. The solid line is the trajectory for the same initial values, labeled by a '◇', as in Fig. 4. The solid and dotted lines are the solutions backward in time from the two initial points labeled by a '□' on the $P = 0$ vertical axis. The unstable interior equilibrium E_{13} is the intersection of the two null-clines (dashed lines).

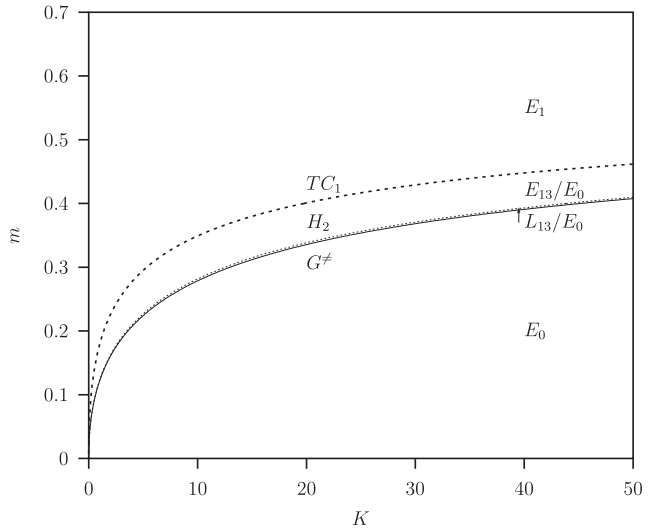

Fig. 6. Two-parameter diagram for the parameters carrying capacity, K, and the natural mortality, m, of demographic PF system (9). All parameter values are given in Table 1. Table 3 gives a list of the bifurcations and see also Fig. 2 where the asymptotic states for P and F are shown varying m where $K = 20$.

is the trajectory for the same initial values, labeled by a '◇', as in Fig. 4. These plots show that for all initial values the solution converges to the origin, whereby first the prey goes extinct in finite time (terminating on the vertical axis) and then the predator disappears asymptotically.

In order to substantiate this statement we simulated the system backward in time starting from points where $P(0) = 0$ and $F(0) > 0$. Two of these trajectories are shown in Fig. 5 starting from points labeled by the '□' symbol. Both terminate at the interior equilibrium point E_{13}. The curve with $F(0) = 0.2925$ is special in the sense that starting below this point where $P(0) = 0$ again, the trajectory goes directly toward the equilibrium without intersecting the P-null-cline above the equilibrium. On the other hand starting above this point the intersection occurs, as for the upper curve with $F(0) = 0.9358$ where the time-backward curve intersects the '◇' point before it lands on the interior equilibrium point E_{13}. There is also an initial condition where the trajectory lands on equilibrium E_1 (not shown). Starting above this point leads to unbounded solutions for $t \to -\infty$.

For $m = 0.278745$ the stable manifold W_0^s is the separatrix between two attractors namely the interior limit cycle L_{13} and the equilibrium E_0. The separatrix is the common boundary of the basins of attraction of the two attractors E_0 and L_{13}. The stable manifold is also invariant and therefore no trajectory can cross this manifold. For $m = 0.05$, however, equilibrium E_0 is globally attracting. Therefore, there is a switching point when m is continued from $m = 0.278745$ to 0.05 where the separatrix disappears. This happens at the global bifurcation where the limit cycle is broken into two non-smooth connected parts: from E_0 to E_1 and from E_1 to E_0. The part on the boundary is the straight line between E_0 and E_1 where $F = 0$ and the interior part where $F > 0$ is the heteroclinic connection where the trajectory starting from E_1 lands exactly in the origin E_0. In that situation the stable manifold W_0^s is precisely also the null-cline connecting E_1 with E_0 where the stable manifold terminates. At that critical parameter value the basin of attraction of the limit cycle finishes and the separatrix between the attractor E_0 and the interior limit cycle L_{13} disappears.

In Fig. 6 the two-parameter diagram is shown for the predator–prey system PF, where both m and K are varied simultaneously. The transcritical bifurcation TC_1 separates regions where we have $E_1 \Rightarrow E_{13}$, the Hopf bifurcation H_2 where $E_{13} \Rightarrow L_{13}$, and the global bifurcation $G^{\neq}$ where $L_{13} \Rightarrow E_0$. In Figs. 3 and 5 the phase plane plot are given for three points in this two-parameter diagram. In Fig. 3a the parameter combination $K = 10,\ m = 0.3$ is a point in Fig. 6 between the curves TC_1 and H_2 where equilibrium E_{13} is stable. In Fig. 3b the parameter combination $K = 10,\ m = 0.278745$ is a point between the curves H_2 and $G^{\neq}$ where limit cycle L_{13} is stable. In Fig. 4 where $K = 1,\ m = 0.05$ is a point in Fig. 6 that lies below the curve $G^{\neq}$ where E_0 is globally stable.

In summary: for low mortality rates the system collapses always completely. For intermediate mortality rates there is bistability between the equilibrium E_0 and equilibrium E_{13}, limit cycle L_{13}, and for higher mortality rates equilibrium E_1. This is indicated in the phase plane plots of Figs. 3 and 5. The boundaries of the basins of attractions (separatrix points) form the switching points in the phase space ($P, F > 0$) to which attractor the system will converge: interior attractor or a total collapse. Note that for $F = 0$ there is no positive P where such a switch occurs like in models with an Allee effect.

In the next section we use these results for comparison with the results of the model where the prey is also suffering from the disease.

5. The predator–prey model with abandoned diseased prey

We study the main three-dimensional system formulated in (2) which is recalled here for the convenience of the reader.

$$\frac{dP}{dt} = P\left(1 - \frac{P^2}{a^2KT^2}\right) - \frac{1}{\lambda}\frac{a^2T}{1+P}F - \frac{1}{2r}PI, \tag{17a}$$

$$\frac{dI}{dt} = 2I\left(\frac{\lambda}{2a^2rT^2}P^2 - bF - \mu\right), \tag{17b}$$

$$\frac{dF}{dt} = \frac{F}{r}\left(\frac{1}{T}\frac{e}{1+P}P + ebI - m\right). \tag{17c}$$

We recall that when $F = 0$ we have system PI (3) and when $I = 0$ system PF (9).

In the next subsections we discuss the equilibria and their stability. Table 4 summarizes the equilibria and Table 5 their stability for the subsystems and the full system.

Table 4
Equilibria for the subsystems and the full system.

Cases	Equilibria	System
(0, 0, 0)	$E_0 = (0, 0, 0)$	
(+, 0, 0)	$E_1 = (aT\sqrt{K}, 0, 0)$	*P*
	$E_{12} = \left(\widetilde{P}_2 = aT\sqrt{2\mu r}, \widetilde{I}_2 = \frac{2r(\lambda K - 2\mu r)}{\lambda K}\right)$	
(+, +, 0)	Eq. (4)	*PI*
	feasible for: $\lambda > \frac{2r\mu}{K}$	
	$E_{13} = \left(\widehat{P}_3 = \frac{mT}{e-mT}, \widehat{F}_3 = m\lambda e\frac{a^2K(e-mT)^2 - m^2}{a^4K(e-mT)^4}\right)$	
(+, 0, +)	Eq. (10)	*PF*
	feasible for: $e \geq mT$ and $m \leq \frac{ae\sqrt{K}}{1+aT\sqrt{K}}$	
	$E_{123} = \left(P_4, I_4 = \frac{mT(1+P_4) - eP_4}{ebT(1+P_4)}, F_4 = \frac{\lambda P_4^2 - 2r\mu a^2T^2}{2rba^2T^2}\right)$	
(+, +, +)	Eq. (22)	*PIF*
	P_4 solution of	
	$\frac{1}{a^2KT^2}\left(P_4^4 + P_4^3\right) + \left(\frac{m}{2reb} - 1\right)\left(P_4^2 + P_4\right) - \frac{a^2T\mu}{\lambda b} = 0$	

5.1. *Equilibria:* PIF-*system*

The equilibria $E_k = (P_k, I_k, F_k)$ are found as follows. We have: the origin $E_0 = (0, 0, 0)$, $E_1 = (aT\sqrt{K}, 0, 0)$ the healthy-prey-only equilibrium, the disease-free predator–prey case equilibrium $E_{13} = (P_2, 0, F_2)$, the endemic predator-free equilibrium $E_{12} = (P_3, I_3, 0)$ and possibly the endemic predator–prey case $E_{123} = (P_4, I_4, F_4)$. The endemic predator-free prey and the disease-free equilibrium of the two-dimensional subsystems were already discussed in the previous section. The introduction of the extra state variable to obtain the three-dimensional system does not change the previous equilibrium results: only, the extra state variable is zero.

For the predators-free endemic prey equilibrium E_{12} we have, see (4)

$$P_2 = aT\sqrt{2\mu r}\,, \quad I_2 = \frac{2r(\lambda K - 2\mu r)}{\lambda K}\,, \quad F_2 = 0\,, \tag{18}$$

with feasibility condition (see (5))

$$\lambda \geq \frac{2\mu r}{K}\,. \tag{19}$$

For the disease-free predator–prey system we have equilibrium E_{13}, see (10)

$$P_3 = \frac{mT}{e - mT}\,, \quad I_3 = 0\,, \quad F_3 = m\lambda e\frac{a^2K(e-mT)^2 - m^2}{a^4K(e-mT)^4}\,, \tag{20}$$

with feasibility condition (see (11))

$$e \geq mT\,, \quad m \leq \frac{ae\sqrt{K}}{1 + aT\sqrt{K}} = m^\dagger\,. \tag{21}$$

For coexistence, solving the second and third equilibrium equation of the system (17), we have

$$F_4 = \frac{\lambda P_4^2 - 2r\mu a^2T^2}{2rba^2T^2}, \quad I_4 = \frac{mT(1+P_4) - eP_4}{ebT(1+P_4)}\,, \tag{22}$$

and for determining P_4 we have the fourth degree polynomial equation

$$\frac{1}{a^2KT^2}\left(P_4^4 + P_4^3\right) + \left(\frac{m}{2reb} - 1\right)\left(P_4^2 + P_4\right) - \frac{a^2T\mu}{\lambda b} = 0\,.$$

Substitution of this expression into (22) gives the expression for I_4 and F_4 just in terms of the parameters.

Descartes' rule of signs tells us the number of roots with positive and negative real parts. For $m > 2reb$, $m = 2reb$ and $m < 2reb$

Table 5
Stability, $\mathrm{tr}(\widehat{\mathbf{J}})$ and $\det\widehat{\mathbf{J}}$ are given in (30) and the equilibria for the *PI* system P_2, I_2 in (18) and for the *PF* system P_3, F_3 in (20).

Equilibria	Eigenvalues	Stability conditions
$\widetilde{E}_0$	$\begin{cases}\widetilde{\omega}_{01} = 1\\ \widetilde{\omega}_{02} = -2\mu\end{cases}$	Always unstable
$\widetilde{E}_1$	$\begin{cases}\widetilde{\omega}_{11} = -2\\ \widetilde{\omega}_{12} = (\lambda K - 2r\mu)/r\end{cases}$	Stable $K < \frac{2r\mu}{\lambda}$
$\widetilde{E}_{12}$	$\begin{cases}\widetilde{\omega}_{21} = 2\frac{-r\mu + \sqrt{r^2\mu^2 - (\lambda K - 2r\mu)\mu\lambda K}}{\lambda K}\\ \widetilde{\omega}_{22} = 2\frac{-r\mu - \sqrt{r^2\mu^2 - (\lambda K - 2r\mu)\mu\lambda K}}{\lambda K}\end{cases}$	Stable $K > \frac{2r\mu}{\lambda}$
$\widehat{E}_0$	$\begin{cases}\widehat{\omega}_{01} = 1\\ \widehat{\omega}_{02} = -m/r\end{cases}$	Unstable saddle
$\widehat{E}_1$	$\begin{cases}\widehat{\omega}_{11} = -2\\ \widehat{\omega}_{12} = -\frac{1}{r}\left(\frac{ea\sqrt{K}}{1+aT\sqrt{K}} - m\right)\end{cases}$	Stable $m < \frac{ae\sqrt{K}}{1+aT\sqrt{K}}$
$\widehat{E}_{13}$	Bifurcation analysis: *PF*-system	Section 4.3
E_0	$\begin{cases}\omega_{01} = 1\\ \omega_{02} = -2\mu\\ \omega_{03} = -m/r\end{cases}$	Unstable saddle
E_1	$\begin{cases}\omega_{11} = -2\\ \omega_{12} = \lambda K/r - 2\mu\\ \omega_{13} = \frac{eaK - m\sqrt{K} - aTKm}{r(\sqrt{K} + aTK)}\end{cases}$	Stable $\begin{cases}m > \frac{ae\sqrt{K}}{1+aT\sqrt{K}}\\ \lambda < \frac{2r\mu}{K}\end{cases}$
E_{12}	$\begin{cases}\omega_{21} = \frac{eP_2}{rT(1+P_2)} + \frac{ebI_2}{r} - \frac{m}{r}\\ \omega_{22,23} = 2\frac{-r\mu \pm \sqrt{r^2\mu^2 - (\lambda K - 2r\mu)\mu\lambda K}}{\lambda K}\end{cases}$	Stable $\left\{m > \frac{eP_2}{T(1+P_2)} + ebI_2\right.$
E_{13}	$\begin{cases}\omega_{31} = \frac{\lambda P_3^2}{ra^2T^2} - 2bF_3 - 2\mu\\ \omega_{32,33} = \frac{1}{2}\left(\mathrm{tr}(\widehat{\mathbf{J}}) \pm \sqrt{\mathrm{tr}(\widehat{\mathbf{J}})^2 - 4\det(\widehat{\mathbf{J}})}\right)\end{cases}$	Stable $\begin{cases}\frac{\lambda}{2ra^2T^2}P_3^2 < bF_3 + \mu\\ \frac{a^2K}{T}\frac{F_3}{(1+P_3)^2} + r < \frac{3rP_3^2}{a^2K}\end{cases}$
E_{123}	Bifurcation analysis: *PIF*-system	Section 5.3

there is only one sign change $++++-$, $++-$ and $++---$ respectively: hence, there is just one positive solution and therefore it must be real and it gives the value of P_4.

With Maple [17] (or other computer programs for symbolic computations) it is possible to derive symbolic expressions for the solutions of the equilibria. However, these expressions are very long and therefore are omitted here.

5.2. *Stability:* PIF-*system*

In contrast to the equilibria values of E_0, E_{12} and E_{13} their stability for the three-dimensional full *PIF*-system has to be determined now anew since the results can be different from those of the two-dimensional *PI* and *PF*-systems derived above.

System *PIF* (17) has the following Jacobian matrix

$$\mathbf{J}=\begin{pmatrix} 1-\frac{3P^2}{a^2T^2K}+\frac{a^2TF}{\lambda(1+P)^2}-\frac{I}{2r} & -\frac{P}{2r} & -\frac{a^2T}{\lambda(1+P)} \\ \frac{2\lambda IP}{ra^2T^2} & \frac{\lambda P^2}{ra^2T^2}-2bF-2\mu & -2bI \\ \frac{eF}{rT(1+P)}-\frac{eFP}{rT(1+P)^2} & \frac{beF}{r} & \frac{eP}{rT(1+P)}+\frac{ebI}{r}-\frac{m}{r} \end{pmatrix}. \tag{23}$$

The origin, equilibrium E_0 of the *PIF*-system (17), is again unstable as it was for the subsystems *PI* and *PF*. The eigenvalues of the Jacobian matrix (23) evaluated at the origin E_0

$$\mathbf{J}_0=\begin{pmatrix} 1 & 0 & -\frac{a^2T}{\lambda} \\ 0 & -2\mu & 0 \\ 0 & 0 & -\frac{m}{r} \end{pmatrix}, \tag{24}$$

are $\omega_{01}=1$, $\omega_{02}=-2\mu$ and $\omega_{03}=-m/r$, showing that E_0 is always an unstable equilibrium. Their respective eigenvectors $\mathbf{v_{0i}}$, $i=1,2,3$ are

$$\mathbf{v_{01}}=\begin{pmatrix}1\\0\\0\end{pmatrix},\ \mathbf{v_{02}}=\begin{pmatrix}0\\1\\0\end{pmatrix},\ \mathbf{v_{03}}=\begin{pmatrix}1\\0\\\frac{\lambda(m+r)}{ra^2T}\end{pmatrix}. \tag{25}$$

Observe that when starting close to the plane $P=0$ in $\mathbb{R}^3_+$, the trajectory converges finally to this equilibrium E_0. The situation is now more complex that in the demographic predator–prey system discussed in Section 4. The stable manifold of E_0 between E_0 and the interior attractors E_{123}, L_{123}, T_{123} is now two dimensional instead of one dimensional. In the sequel we will not calculate this separatrix explicitly.

At equilibrium E_1 we find the following eigenvalues of the Jacobian matrix $\omega_{11}=-2$, $\omega_{12}=\lambda K/r-2\mu$, and $\omega_{13}=(eaK-m\sqrt{K}-aTKm)[r(\sqrt{K}+aTK)]^{-1}$. Thus it is stable for

$$m>\frac{ae\sqrt{K}}{1+aT\sqrt{K}}=m^{\dagger},\quad \lambda<\frac{2r\mu}{K}. \tag{26}$$

At equilibrium E_{12} where $F=0$ the Jacobian matrix reads

$$\mathbf{J}_{12}=\begin{pmatrix} 1-\frac{3P_2^2}{KT^2a^2}-\frac{I_2}{2r} & -\frac{P_2}{2r} & -\frac{a^2T}{\lambda(1+P_2)} \\ \frac{2\lambda I_2P_2}{ra^2T^2} & \frac{\lambda P_2^2}{ra^2T^2}-2\mu & -2bI_2 \\ 0 & 0 & \frac{eP_2}{rT(1+P_2)}+\frac{ebI_2}{r}-\frac{m}{r} \end{pmatrix}, \tag{27}$$

and the eigenvalues are explicitly evaluated as

$$\omega_{21}=\frac{eP_2}{rT(1+P_2)}+\frac{ebI_2}{r}-\frac{m}{r},$$
$$\omega_{22,23}=2\frac{-r\mu\pm\sqrt{r^2\mu^2-(\lambda K-2r\mu)\mu\lambda K}}{\lambda K}.$$

Observe that in view of feasibility (5) both eigenvalues ω_{22} and ω_{23} have negative real parts. Stability is thus ensured only by

$$m>\frac{erP_2}{rT(1+P_2)}+ebI_2$$
$$=\frac{eraT\sqrt{2\mu r}}{rT(1+aT\sqrt{2\mu r})}+ebr\frac{2r(\lambda K-2\mu r)}{\lambda K}, \tag{28}$$

where P_2 and I_2 are given by (18).

At equilibrium E_{13} where $I_3=0$ the Jacobian matrix reads

$$\mathbf{J}_{13}=\begin{pmatrix} 1-\frac{3P_3^2}{a^2T^2K}+\frac{a^2TF_3}{\lambda(1+P_3)^2} & -\frac{P_3}{2r} & -\frac{a^2T}{\lambda(1+P_3)} \\ 0 & \frac{\lambda\widehat{P}_3^2}{ra^2T^2}-2bF_3-2\mu & 0 \\ \frac{eF_3}{rT(1+P_3)}-\frac{eF_3P_3}{rT(1+P_3)^2} & \frac{beF_3}{r} & \frac{e\widehat{P}_3}{rT(1+P_3)}-\frac{m}{r} \end{pmatrix}. \tag{29}$$

One eigenvalue factors out, namely

$$\omega_{31}=\frac{\lambda P_3^2}{ra^2T^2}-2bF_3-2\mu.$$

The remaining 2×2 minor $\widehat{\mathbf{J}}$ is the matrix of the *PF*-system given in (12) evaluated now for $P=P_3$ and $F=F_3$. The eigenvalues are

$$\omega_{32,33}=\frac{1}{2}(\mathrm{tr}(\widehat{\mathbf{J}})\pm\sqrt{\mathrm{tr}(\widehat{\mathbf{J}})^2-4\det(\widehat{\mathbf{J}})}).$$

The Routh–Hurwitz sufficient condition for asymptotic stability becomes

$$\mathrm{tr}(\widehat{\mathbf{J}})=r\left(1-\frac{3P_3^2}{a^2K}\right)+\frac{a^2K}{T}\frac{1}{(1+P_3)^2}F_3<0,$$
$$\det(\widehat{\mathbf{J}})=\frac{2e}{T^2}\frac{a^2K}{(1+P_3)^3}F_3>0. \tag{30}$$

The second condition obviously holds, so that stability of E_{13} is guaranteed if

$$\frac{\lambda}{2ra^2T^2}P_3^2<bF_3+\mu,\quad \frac{a^2K}{T}\frac{F_3}{(1+P_3)^2}+r<\frac{3rP_3^2}{a^2K}. \tag{31}$$

For the other equilibria, with symbolic manipulators it is possible to compute the expressions for the eigenvalues of the Jacobian matrix evaluated at E_{123} in terms of parameters and to derive stability criteria. However, these expressions are intractable. Furthermore it is not possible to perform a symbolic analysis in the case of limit cycles (and in general for chaos) or phenomena related to global bifurcations. This holds also for the situations when extinction of one of the populations occurs in finite time. In order to complete the study we perform a numerical bifurcation analysis using the parameter values given in Table 1.

5.3. *Bifurcation analysis:* PIF-*system*

In Fig. 7 the two-parameter diagram is shown for the endemic predator–prey system *PIF*, where both m and K are varied simultaneously. The three bifurcation curves for the disease-free system, TC_1, H_2 and $G^{\neq}$, were already discussed among the results presented in Fig. 6. Before we start the analysis we point out that everywhere in this diagram E_0 will also be an attractor when starting close to the plane $P=0$ where $F>0$ and $I>0$. However, in the diagrams we indicate only the additional interior attractors. Firstly,

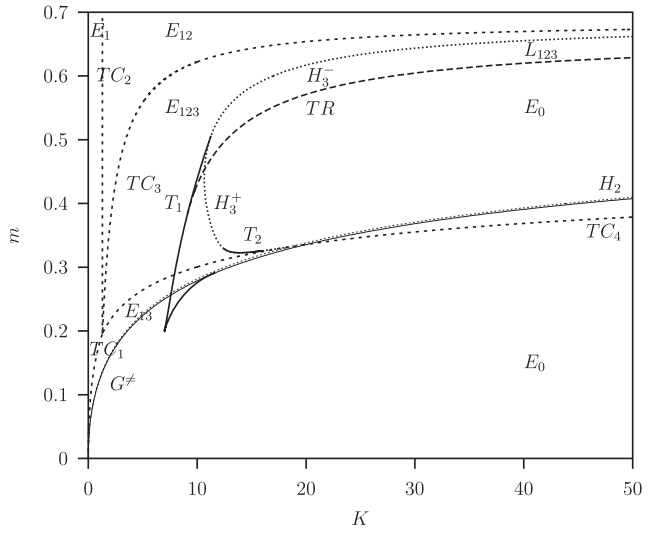

Fig. 7. Two-parameter diagram in terms of the parameters K, the carrying capacity, and m, the natural mortality, of the *PIF* ecoepidemic system (17) with $I = 0$. All parameter values are given in Table 1. Table 2 gives a list of the asymptotic dynamics and Table 3 gives a list of the bifurcations.

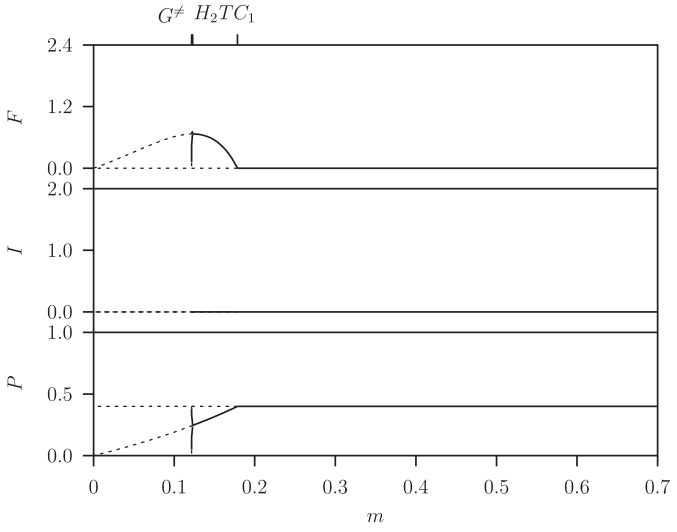

Fig. 9. One-parameter bifurcation diagram for the ecoepidemic *PIF* system (17) for the susceptible prey population, P, the infected prey population I, and the predator population, F with free parameter m where $K = 1$. See Fig. 2 for a description of the symbols.

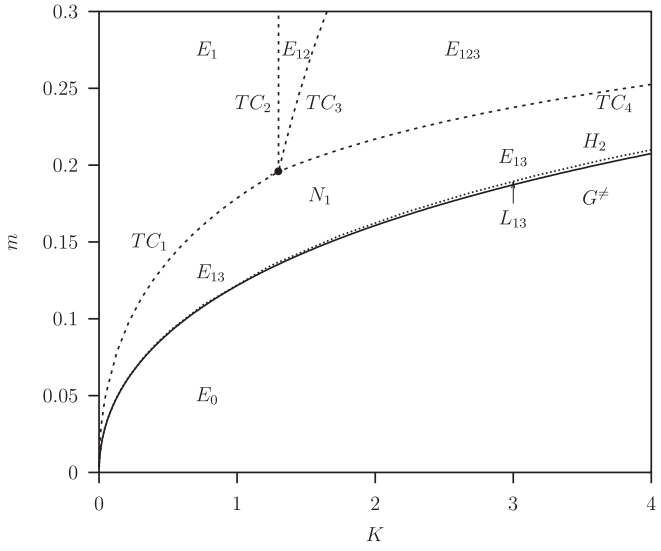

Fig. 8. Two-parameter diagram for parameters carrying capacity, K, and natural mortality, m, of the ecoepidemic *PIF* system (17). This is a blow up of the diagram presented in Fig. 7 for the range $0 \le K \le 4$.

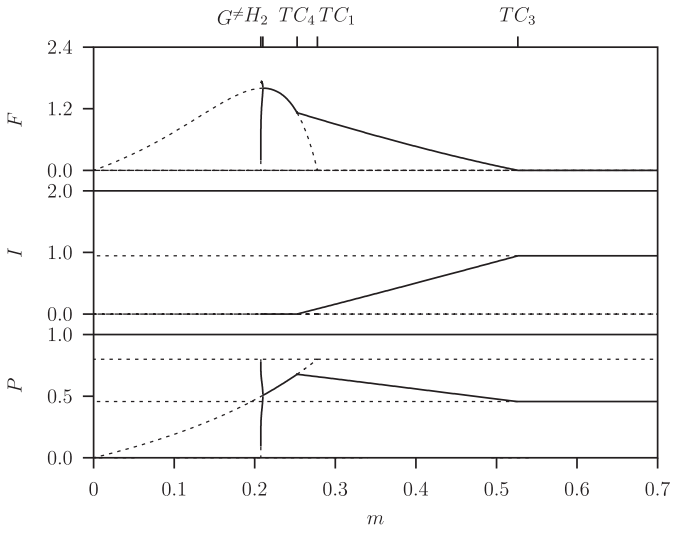

Fig. 10. One-parameter bifurcation diagram for the ecoepidemic *PIF* system (17) showing the susceptible prey population, P, the infected prey population I, and the predator population, F with free parameter m where $K = 4$. See Fig. 2 for a description of the symbols.

the healthy prey population goes extinct in finite time and thereafter the infected prey and predator populations asymptotically.

We split up the analysis in three different ranges for the parameter K, the low range $0 < K < 4$, the intermediate one $0 < K < 20$, and the high range $K \ge 20$.

5.3.1. Low carrying capacity $0 \le K \le 4$ analysis: PIF-*system*

We start our description of the long-term dynamics of the system for small values of K. A blow up of the two-parameter diagram presented in Fig. 7 is shown for the range $0 \le K \le 4$ in Fig. 8.

The transcritical bifurcation TC_1 between the origin E_0 and a codimension-two point N_1 separates the parameter space between the two equilibria E_1 and E_{13}. This is clear from Fig. 9 where the long-term state variable values are plotted for fixed $K = 1$ and varying m. Above the transcritical bifurcation TC_1 only the healthy prey population exists at equilibrium E_1. Between TC_1 and the Hopf bifurcation H_2 the predator and disease-free prey exist at equilibrium E_{13}. Below the H_2 the maximum and minimum values for the stable limit cycle L_{13} are plotted till the collapse of the complete system at the global bifurcation point $G^{\neq}$.

With increasing K and m from point N_1 in Fig. 8, three new transcritical bifurcations TC_2, TC_3 and TC_4 emerge. At TC_2 the prey population becomes infected, namely a predator-free system *PI* arises: the equilibrium E_{12} appears consisting of susceptible and infected sub-populations. Furthermore at both TC_3 and TC_4 the infected prey invades forming the system *PIF* with interior positive equilibrium E_{123} from the subsystems *PI* and *PF* respectively. Fig. 10, where $K = 4$ (instead of $K = 1$ in Fig. 9), illustrates the latter case with the transition from *PF* to *PIF* at TC_4.

5.3.2. Intermediate carrying capacity $4 \le K < 20$ analysis: PIF-*system*

Fig. 11 is also an enlargement of a part of the two-parameter diagram of Fig. 7 for $0 \le K \le 20$. The interior equilibrium E_{123} of the *PIF*-system becomes unstable at the Hopf bifurcation curve H_3. This Hopf bifurcation can be supercritical, denoted by H_3^-, giving rise

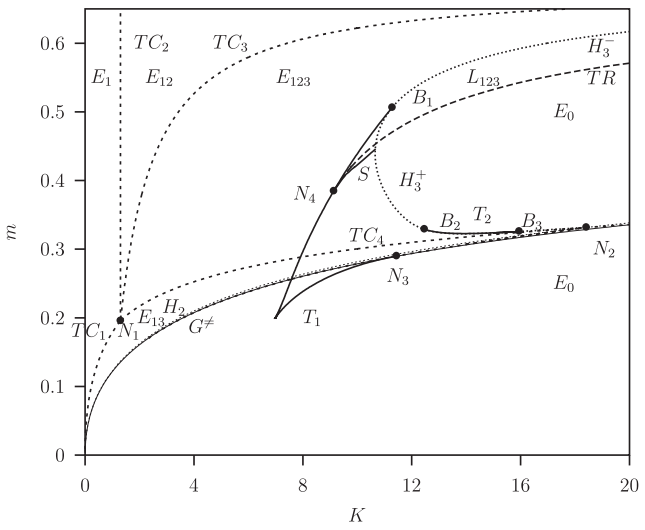

Fig. 11. Two-parameter diagram for parameters carrying capacity, K, and natural mortality, m, of the ecoepidemic *PIF* system (17). This is a blow up of the diagram presented in Fig. 7 in the range $0 \le K \le 20$. Note that in the (small) region between the tangent T_1 between B_1 and N_4, the torus bifurcation TR starting in N_4 and the Hopf bifurcation H_3^+ between B_1 and B_2 there is tri-stability of a stable equilibrium E_{123} a stable limit cycle L_{123} and E_0. Table 2 gives a list of the asymptotic dynamics and Table 3 gives a list of the bifurcations.

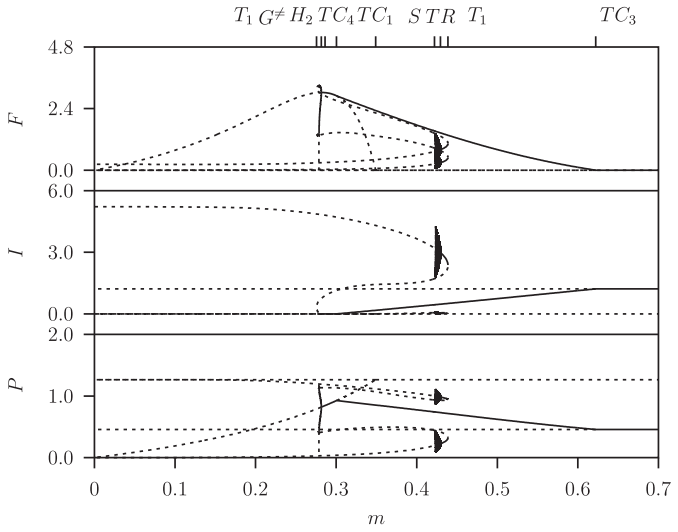

Fig. 12. One-parameter bifurcation diagram for the ecoepidemic *PIF* system (17) showing the susceptible prey population, P, the infected prey population I, and the predator population, F with free parameter m where $K = 10$. All the other parameter values are given in Table 1. The solid (dashed) curves denote stable (unstable) equilibrium values. The limit cycle L_{123} is stable between tangent T_1 and torus TR bifurcations and between TR and the torus destruction bifurcation S there is the quasi-periodic torus dynamics T_{123}. Note that these regions are very narrow. Above TC_4 the prey is infected. Below TC_3 the predator invades the healthy and diseased prey. Table 3 gives a list of the bifurcations.

to a stable limit cycle L_{123}, or subcritical, then denoted by H_3^+, in which case the originating limit cycle L_{123} is unstable. At three so called Bautin (or Generalised-Hopf) bifurcation points, denoted by B_i, $(i = 1, 2, 3)$ where the switch from super- to subcritical or vice versa, takes place continuing the Hopf bifurcation, tangent bifurcation curves for limit cycles, T_i, $(i = 1, 2)$ emerge (Fig. 11). At $K = 20$ the Hopf is supercritical (a stable limit cycle originates). Following the Hopf curve H_3^- by lowering K, at the first Bautin point B_1 it becomes subcritical. The originating tangent bifurcation curve for limit cycles, T_1, goes via a cusp to the global bifurcation curve $G^{\neq}$ curve. It terminates there at a point N_3 where there are no infected prey, $I = 0$, and where the system reduces to the *PF*-system and merges there with the curve $G^{\neq}$ of *PF*-system shown in Fig. 6.

Continuing on the Hopf curve H_3^+ in Fig. 11 again from point B_1, first the Hopf curve H_3^+ becomes supercritical at the Bautin point B_2, then changes again feature and becomes once more subcritical at B_3. Between the two Bautin points B_2 and B_3 there is a tangent bifurcation T_2 above the supercritical Hopf bifurcation curve H_3^- (this supercritical Hopf bifurcation curve is not labeled in Fig. 11). Continuing from B_3, the Hopf curve terminates also at the point N_2 where there are no infected prey, $I = 0$, and where the system reduces to the *PF*-system. At that point it merges with the Hopf bifurcation H_2 of the *PF*-system shown in Fig. 6.

In the region bounded by the Hopf bifurcation curve in Fig. 11 there is a torus bifurcation TR where the stable limit cycle L_{123} becomes unstable. This torus bifurcation curve terminates at point N_4 on the tangent bifurcation curve T_1. In the very small region bounded by the tangent T_1 between B_1 and N_4, the torus bifurcation TR starting at N_4 and the Hopf bifurcation H_3^+ between B_1 and B_2 there is tri-stability of a stable equilibrium E_{123} and a stable limit cycle L_{123} and zero equilibrium E_0.

This is explained by showing results of continuation studies presented in Fig. 12 where $K = 10$ and varying m and Fig. 13 where $m = 0.42$ and varying K.

Comparison of the diagrams of Figs. 12 and 10 where $K = 4$ instead of $K = 10$ shows the new dynamics related to the periodic solutions, where $I > 0$ in the region $0.4 < m < 0.5$. We follow the maximum values of I curve starting from the heteroclinic connection point $G^{\neq}$ at $m = 0.2862$. Decreasing m gives a tangent bifurcation curve T_1 at $m = 0.2757$ and then increasing at $m = 0.43884$ a new point on the tangent bifurcation curve T_1 is found. Except close the second T_1 point, the limit cycle is unstable. The small region where it is stable is bounded by T_1 at $m = 0.43884$ and a torus bifurcation TR at $m = 0.42938$. The origin of the limit cycles and what happens below the TR will be explained now by studying the results in Fig. 13.

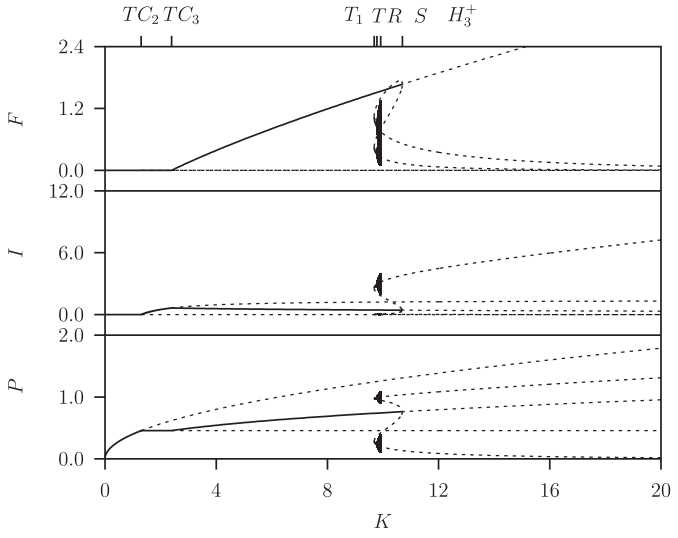

Fig. 13. One-parameter bifurcation diagram for the ecoepidemic *PIF* system (17) showing the susceptible prey population, P, the infected prey population I, and the predator population, F with free parameter K where $m = 0.42$. Note that the stable limit cycle between T_1 and TR and the quasi-periodic torus dynamics between TR and S described in the text, are hardly apparent, in view of the fact that it exists in the very narrow region. Table 3 gives a list of the bifurcations.

Fig. 13 shows the bifurcation sequence for increasing K till $K = 20$ where $m = 0.42$ (see also Fig. 11 again). Starting from say $K = 0$ firstly part of the healthy prey populations in equilibrium becomes infected at the transcritical TC_2 bifurcation. Increasing K at TC_3 the

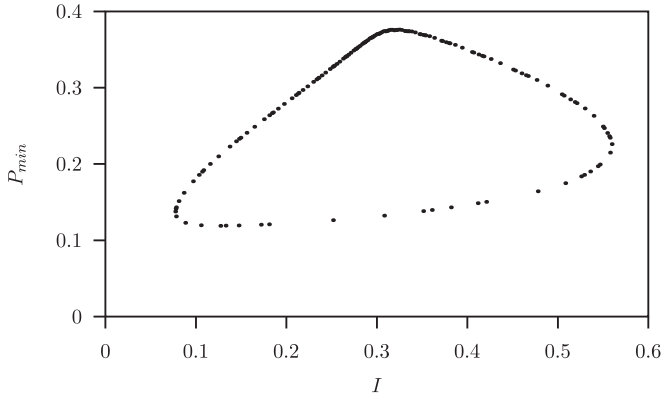

Fig. 14. Minimum map for the susceptible prey $P_{\min}$ versus the infected prey I for $m = 0.42$. The parameter K is close to the right of the torus bifurcation TR. Note that for longer times the dots form approximately a closed curve in the Poincaré plane where $dP/dt = 0$.

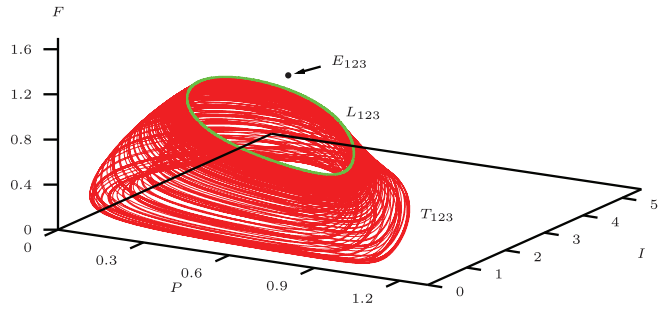

Fig. 15. Solution plot in the susceptible prey P, infected prey I and predator F phase space for $m = 0.42$ and at a point just below S for $K = 9.91496$ on the quasi-periodic torus attractor T_{123} depicted in red, at point above of the torus bifurcation TR. Also in green the saddle limit cycles is shown that emerges from the subcritical Hopf bifurcation H_3^+ at $K = 10.6978$ in Fig. 13. (For interpretation of the references to color in this figure legend, the reader is referred to the web version of this article.)

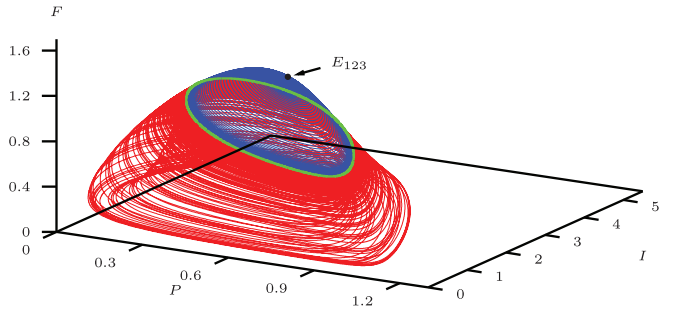

Fig. 16. Solution plot in the susceptible prey P, infected prey I and predator F phase space for $m = 0.42$ and just above point S for $K = 9.91596$ on the quasi-periodic torus attractor T_{123} at point above of the torus bifurcation TR. (For interpretation of the references to color in this figure legend, the reader is referred to the web version of this article.)

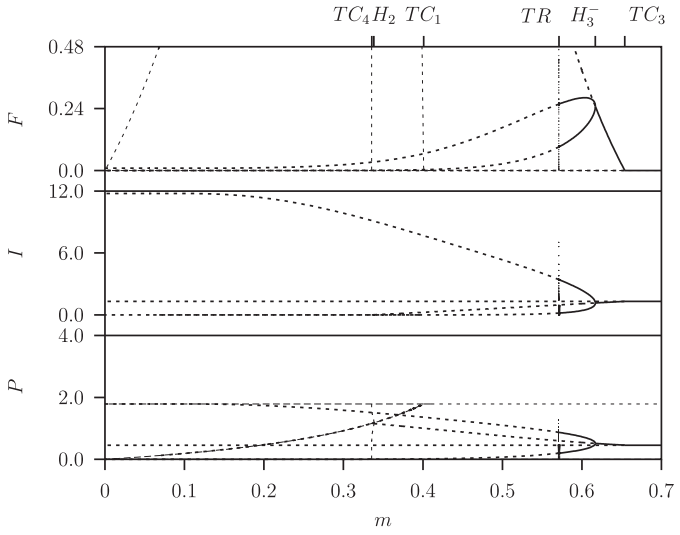

Fig. 17. One-parameter bifurcation diagram for the ecoepidemic *PIF* system (17) showing the susceptible prey population, P, the infected prey population I, and the predator population, F with free parameter m where $K = 20$. All other parameter values are given in Table 1. The solid (dashed) curves denote stable (unstable) equilibrium values. Table 3 gives a list of the bifurcations.

predator population enters into the system and starts to feed on the two prey sub-population. Here, there is coexistence between two attractors E_0, E_{123}. This stable interior equilibrium E_{123} becomes unstable at a subcritical Hopf bifurcation H_3^+ at $K = 10.6978$. The originating limit cycle is unstable and coexists with the stable equilibrium. This unstable limit cycle becomes stable at a tangent bifurcation T_1. In this region there is coexistence between three attractors E_0, L_{123} and E_{123}. Following this stable branch the limit cycle becomes unstable at the torus bifurcation TR.

This torus bifurcation TR occurs with $m = 0.42$ at $K = 9.68296$. The dynamics on the torus emerging from this torus bifurcation with increasing K is quasi-periodic (characterized by two Lyapunov exponents equal zero). This can be shown by plotting the points where the trajectory intersects the Poincaré plane for $dP/dt = 0$ (see Fig. 14). The dots in the graph form closed curves when simulations continue for longer times and hence show quasi-periodic dynamics on the torus (which we will call for short torus dynamics, denoted by T_{123}). Fig. 15 shows the attractor T_{123} in the phase-space for the three state variables on the torus for $K = 9.91496$. In Fig. 13 also the saddle limit cycle which originated from subcritical Hopf bifurcation H_3^+ at $K = 10.6978$ is shown. Hence in this region there is coexistence between three attractors E_0, T_{123} and E_{123}.

When we continue following the quasi-periodic torus attractor T_{123} with increasing K this torus dynamics is destructed at a point labeled S by the saddle limit cycle that emerges at the subcritical Hopf bifurcation H_3^+ at $K = 10.6978$. This phenomenon occurs between $K = 9.91496$ and 9.91596 (see Figs. 15 and 16). This bifurcation point is denoted by S. In Fig. 15 where $K = 9.91496$ starting on the torus, the dynamics remains on the torus while during time intervals the trajectory is close to the saddle limit cycle depicted in green.

In Fig. 16 where $K = 9.91596$ on the other hand, starting on the torus shown in Fig. 15 where $K = 9.91496$, firstly the dynamics in red follows closely the torus dynamics but after passing the saddle cycle, depicted in green, it converges in blue toward the stable equilibrium E_{123}. Together with the torus dynamics also its basin of attraction disappears at the transition point. In other words the stable manifold associated with the saddle limit cycle loses its function as a separatrix between T_{123} and E_{123}. Hence, beyond this bifurcation point S there is only coexistence between E_0 and E_{123}.

Here we considered the case where the stable equilibrium E_{123} exists, that is for K values below H_3^+ in Fig. 11. Then, in the interval between the tangent T_1 and the torus bifurcation TR there can occur several possibilities: tri-stability of the stable equilibrium E_{123} and the stable limit cycle L_{123} and a collapse of the whole system to equilibrium E_0 after the prey population becomes extinct in a finite time. Between TR and S the stable limit cycle L_{123} is replaced by the quasi-periodic torus attractor T_{123}. Beyond S there is bistability of E_{123} and E_0.

However, in the region above the Hopf bifurcation $H_3^{\pm}$ the interior equilibrium E_{123} is unstable, see Fig. 11. In the next section

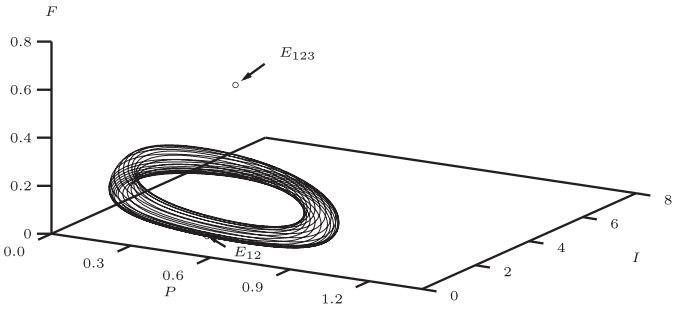

Fig. 18. Solution plot in the susceptible prey, *P*, infected prey, *I*, predator, *F*, phase space for $m = 0.5711$ close below the torus bifurcation *TR* where the solution is quasi-periodic T_{123} and $m = 0.571$ (dashed curve) close below to the torus bifurcation *TR* where the solution converges to the zero-state solution.

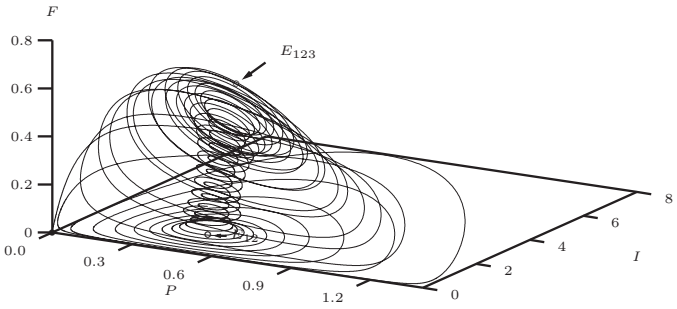

Fig. 19. Solution plot in the susceptible prey, *P*, infected prey, *I*, predator, *F*, phase space for $m = 0.57109$ close below the torus bifurcation *TR* where the solution is quasi-periodic T_{123}. Also the two unstable equilibria E_{12} and E_{123} are shown. Eventually there is a collapse of the whole system.

we will study the dynamics of the system in this region in Fig. 7. These results will be important for higher carrying capacities.

5.3.3. High carrying capacity K ≥ *20 analysis:* PIF-*system*

For a high carrying capacity keeping $K = 20$ fixed in Fig. 17 (instead of $K = 10$ in Fig. 12) we give the one-parameter diagram by varying *m*.

Starting with a high mortality rate, say $m = 0.7$ above the transcritical bifurcation TC_3, the prey-only diseased system exists stably. Decreasing *m* at TC_3 the predator invades the system and the interior equilibrium E_{123} is stable. It becomes unstable crossing the supercritical Hopf bifurcation H_3^- and an interior stable limit cycle L_{123} emerges. Lowering *m* further this limit cycle becomes unstable at the torus bifurcation *TR*. It appears that the dynamics on the emerging torus is quasi-periodic. This dynamics is shown in Fig. 18 for $m = 0.628$, a value slightly below the torus bifurcation *TR* for $m = 0.629$.

Decreasing *m* further shows a very sudden change of the dynamics. The amplitude of the oscillations grow and also the final shape of the trajectory changes drastically. This is shown in Fig. 19 where $m = 0.57109$. We started simulations in time with initial values on the torus shown in Fig. 19 for $m = 0.5711$ and then first slowly in time the trajectory changes drastically. The amplitude especially in the *F* direction increases and during the oscillatory dynamics the trajectory passes the origin closely and finally the system collapses, first *P* in finite time and thereafter *F* and *I* exponentially. Observe that the collapse of the system is unrelated to a destruction by a saddle limit cycle as we saw in Fig. 16.

What occurs is more similar to what happened in the case of the two-dimensional *PF* system when the heteroclinic orbit was approached, see Fig. 3 where the vector field for $K = 10$ with $m = 0.278745$ was shown. That trajectory ended in the stable limit cycle L_{13} but for lower values this limit cycle was broken and the system collapses as in Fig. 5. At the switching point the trajectory lands exactly in the origin. In that situation the stable manifold W_0^s terminates being a separatrix so that E_0 becomes a global attractor.

However, the situation for the three-dimensional *PIF* system differs much from that in the two-dimensional *PF* system due to the fact that the interaction between the infected and the predators with the healthy prey differs, see Sections 3 and 4. Now when the trajectory approaches the zero equilibrium, not only *F* becomes small but *I* also. This was shown in Fig. 1 for the *PI*-system and for the *PF*-system Figs. 3 and 5. The vector field in the three-dimensional state space close to the origin is shown in Fig. 20 for $m = 0.57109$ and $K = 20$.

When both *F* and *I* get small (blue and green arrows) the trajectory remains close to the $F = 0$ and $I = 0$ plane where *P* increases (red arrows) toward the saddle equilibrium E_1. Thereafter by increasing *I* and to a much lesser extent *F* it approaches as a spiral close to the *P*–*I* plane the unstable prey-only equilibrium E_{12}. Indeed condition (28) is not satisfied at this point while the real

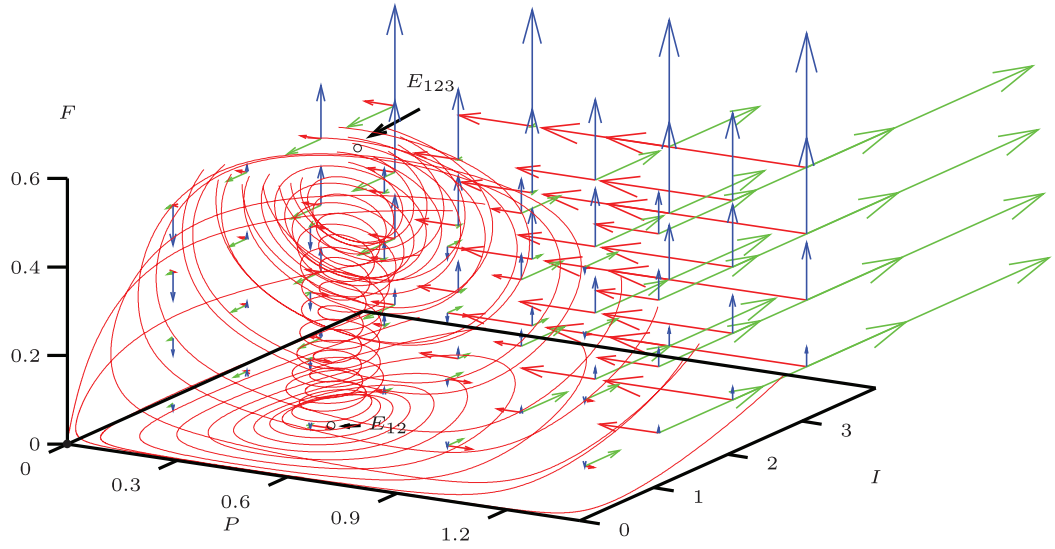

Fig. 20. Vector field plot in the susceptible prey, *P*, infected prey, *I* and predator *F* phase space for $m = 0.57109$ and $K = 20$. See also Fig. 19 for the description of the dynamics. (For interpretation of the references to color in this figure legend, the reader is referred to the web version of this article.)

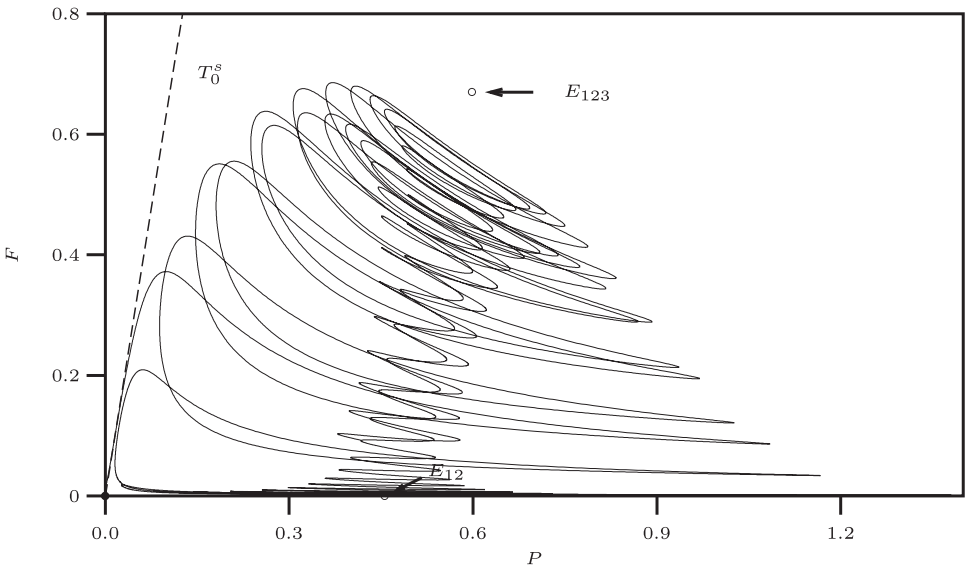

Fig. 21. Projection plot of Fig. 19 in the susceptible prey, P, predator, F, phase space for $m = 0.57109$ and $K = 20$. Also the linear tangent manifold T_0^s is shown. This line is crossed before the total collapse occurs with convergence to the zero equilibrium E_0 in the origin.

parts of the eigenvalues ω_{22} and ω_{23} are negative. However, close to E_{12} the predator population F increases sharply and the trajectory spirals with relatively small amplitude in the P–I plane toward the unstable interior equilibrium E_{123}. Now the amplitude of the oscillatory dynamics in the P–I plane grow while the predator size F decreases again. So, there is a kind of torus dynamics. But for all m values where the quasi-periodic solution was not stable, we found a total collapses of the system where first the healthy prey become extinct in finite time and thereafter the infected prey and predator.

The projection of the trajectory of Fig. 20 is shown in Fig. 21. This plot shows that just before collapsing the trajectory crosses the linear tangent manifold T_0^s and by assumption also the stable manifold W_0^s which does not act as a separatrix anymore. Since we found this for all values below the point where the quasi-periodic torus dynamics became unstable (the extra zero Lyapunov exponent became positive) this point is catastrophic in the sense that below this curve in the two-parameter diagram the system always goes extinct.

6. Discussion and conclusions

The analysis of the prey-only system shows that the prey can be infected when the carrying capacity is above a certain threshold given in (8) independently of the mortality rate of the predator. It depends, however, on the contact rate for the transmissible and unrecoverable disease of the prey.

The demographic predator–prey model shows that the predators invade the system when the prey-only equilibrium becomes unstable, i.e. for a small enough predator mortality rate, see (11). Varying the mortality rate of the predator the predator–prey equilibrium exists whenever the predators' mortality rate falls below a threshold (see Fig. 6). Through the prey carrying capacity, K, the environment always influences that threshold level. The predators too contribute to this phenomenon, since their efficiency in hunting appears in the threshold expression, i.e. through the hunting rate of predator on healthy prey, parameter a. Note that even in the purely demographic model besides the hunting rate the prey capture time T and the conversion factor of prey into predator e appear explicitly in the expression for the threshold (11).

The demographic predator–prey equilibrium becomes unstable with lowering m at a Hopf bifurcation. The amplitude of the originating limit cycle grows very fast and the limit cycle disappears suddenly at a heteroclinic connection in a global bifurcation $G^{\neq}$ from a saddle disease-free prey-only equilibrium point E_1 to the zero-solution E_0 where the total system collapsed. This has already been discussed in [5,8] but this analysis is extended here by a thorough phase portrait analysis in this paper.

The linear stability analysis of the origin shows it to be always unstable, a fact that would guarantee the survival of at least some part of the ecosystem. This would occur also for the disease-free predator–prey model, thereby showing that this ecosystem behavior is due essentially to demographic reasons. The healthy prey reproduction rate provides the positive eigenvalue responsible for the origin instability. However, the study of the phase plane analysis shown in Figs. 3 and 5 reveals the existence of a sector in the phase plane, for which trajectories are doomed to end up into the origin, see Fig. 4 (see also [25]). This indicates that the actual ecosystem behavior is prone to become extinct in the region labeled E_0 in the bifurcation diagram (Fig. 8). In unfavorable circumstances, the prey in fact becomes extinct in finite time, followed by an exponential decay of the predators. This phenomenon is related to the presence of the square root terms in the Holling type II functional response in accordance with the findings of Braza in [5]. Here, however, we stress that our findings further indicate that the phenomenon occurs after the prey population gets extinct in a finite time.

We studied using a phase plane analysis the functioning of the separatrix of two coexisting attractors, the demographic predator–prey equilibrium E_{13} or limit cycle L_{13} and the zero equilibrium E_0 where a total collapse of the system occurred. The relationship with the heteroclinic connection was illustrated. The fact that a stable manifold is invariant disallows that a trajectory crosses this manifold. Hence, the stable manifold loses its separatrix property at the heteroclinic connection where the zero equilibrium becomes a global attractor.

There is resemblance with the dynamics of predator–prey systems with a strong Allee effect (see for instance [22]). There the quadratic logistic is replaced by a cubic growth function of the prey giving three prey-only equilibria instead of two. Also in that

predator–prey systems an unexpected collapse can occur. There this event is referred to as over-exploitation.

The bifurcation analysis reveals an organizing center point N_1 in the two-dimensional parameter space in which K and m are taken as bifurcation parameters (Figs. 7 and 8). Transcritical bifurcations, TC's, show the change in the composition of the system induced by a change in a parameter: these occur when the predator invades a prey equilibrium at TC_1 ($P \Rightarrow PF$) or the prey population becomes infected at TC_2 ($P \Rightarrow PI$). At the transcritical bifurcations TC_3 or TC_4 the prey population becomes infected ($PF \Rightarrow PIF$).

Non-equilibrium, oscillatory dynamic behaviors occur in the two parameter bifurcation diagram for the two parameters K and m. The non-equilibrium solutions emerge at Hopf bifurcations. The pattern of the originating limit cycles shows a cusp bifurcation and this gives rise to more complex dynamics together with the fact that these limit cycles become unstable at a torus bifurcation. Generally this can be the onset of chaotic dynamics. We found however only quasi-periodic dynamics originating from the torus bifurcation.

The way the torus dynamics is destructed by the saddle limit cycle (for instance shown in Figs. 15 and 16), resembles the way a limit cycle is broken by a saddle point giving a homoclinic connection of this saddle to itself (see also [4]). Here it happens in one dimension higher: the point is replaced by a limit cycle and the limit cycle by a quasi-periodic dynamics on a torus (see also [6] for more details). In [3] the destruction by a saddle-cycle, is called a homoclinic bifurcation.

We stress that these results were obtained for the parameter values given in Table 1. Because of the smoothness of the model these results are robust for small perturbations of the other parameters, that are now fixed. For larger deviations, however, the region where complex dynamics occurs can grow or even disappear and furthermore even other complex dynamics may show up. This is inherent in applying a numerical bifurcation analysis. On the other hand, the results obtained for the standard transcritical and Hopf bifurcations remain valid.

A model with diseased predators instead of infected prey was described and analysed in [8, Eq. (14)], with the three state variables: the prey, healthy predators and infected predators. There the topological structure was that of a food chain, namely infected predators have a negative effect on healthy predators and healthy predators on the prey whereby the self-regenerating prey have a negative effect on themselves. The topological structure of the ecoepidemic studied here, system (17), is the one of an ecosystem with omnivory, namely here predators have a negative effect on both infected and healthy prey while infected prey have a negative effect on healthy prey. Hence, the infected prey and the predator are also competitors. The healthy prey population has a negative effect on itself expressed by the logistic growth because they are self-replicating. The resulting bifurcation diagrams respect these topologies (see also [13,14]). There is an organizing center N_1 where the population at the lowest level, the healthy prey, can be invaded by both the other populations, infected prey and predator, either separately or together (see [13, Fig. 11 (left-bottom panel)]). This is the typical invasion of the prey by two predator populations that compete for the prey.

From the two-parameter diagram (Fig. 7) due to the weakening of the prey population by infection we conclude that the predator feeding on the prey population can exist for larger natural mortality rates of predators when prey carrying capacities are sufficient. However, with larger carrying capacities the system starts first to show oscillatory dynamics, a phenomenon related to the "paradox of enrichment" [20], and for higher values a collapse of the system occurs for a wide range of natural mortality rates where the prey population goes extinct in finite time.

References

[1] V. Ajraldi, M. Pittavino, E. Venturino, Modelling herd behavior in population systems, Nonlinear Anal. Real World Appl. 12 (2011) 2319–2338.
[2] A.D. Bazykin, Nonlinear Dynamics of Interacting Populations, World Scientific, Singapore, 1998.
[3] A.M. Bate, F.M. Hilker, Complex dynamics in an eco-epidemiological model, Bull. Math. Biol. 75 (2013) 2059–2078.
[4] A.M. Bate, F.M. Hilker, Disease in group-defending prey can benefit predators, Theor. Ecol. 7 (2014) 87–100.
[5] P.A. Braza, Predator-prey dynamics with square root functional responses, Nonlinear Anal. Real World Appl. 13 (2012) 1837–1843.
[6] S. Chakraborty, B.W. Kooi, B. Biswas, J. Chattopadhyay, Revealing the role of predator interference in a predator-prey system with disease in prey population, Ecol. Complex. 21 (2015) 100–111.
[7] C. Cosner, D.L. DeAngelis, J.S. Ault, D.B. Olson, Effects of spatial grouping on the functional response of predators, J. Theor. Biol. 56 (1999) 65–75.
[8] G. Gimmelli, B.W. Kooi, E. Venturino, Ecopidemic models with prey group defense and feeding saturation, Ecol. Complex. 22 (2015) 50–58.
[9] E.J. Doedel, B. Oldeman, Auto 07p: Continuation and bifurcation software for ordinary differential equations, Technical report, Concordia University, Montreal, Canada, 2009.
[10] H.I. Freedman, G.S.K. Wolkowicz, Predator-prey systems with group defense: The paradox of enrichment revisited, Bull. Math. Biol. 48 (1986) 493–508.
[11] S.A.H. Geritz, M. Gyllenberg, Group defence and the predator's functional response, J. Math. Biol. 66 (2013) 705–717.
[12] J. Guckenheimer, P. Holmes, Nonlinear Oscillations, Dynamical Systems and Bifurcations of Vector Fields, Applied Mathematical Sciences vol. 42, 2nd ed., Springer-Verlag, New York, 1985.
[13] B.W. Kooi, L.D.J. Kuijper, M.P. Boer, S.A.L.M. Kooijman, Numerical bifurcation analysis of a tri-trophic food web with omnivory, Math. Biosci. 177-178 (2002) 201–228.
[14] B.W. Kooi, Numerical bifurcation analysis of ecosystems in a spatially homogeneous environment, Acta Biotheor. 51 (2003) 189–222.
[15] Y.A. Kuznetsov, Elements of Applied Bifurcation Theory, Applied Mathematical Sciences vol. 112, 3rd ed., Springer-Verlag, New York, 2004.
[16] H. Malchow, S. Petrovskii, E. Venturino, Spatiotemporal Patterns in Ecology and Epidemiology, CRC, Boca Raton, 2008.
[17] Maple software, 2008, Maplesoft, Waterloo, ON, Canada.
[18] MATLAB package, 2014, The MathWorks, Natick, Massachusetts, USA.
[19] M.L. Rosenzweig, R.H. MacArthur, Graphical representation and stability conditions of predator-prey interactions, Am. Nat. 97 (1963) 209–223.
[20] M.L. Rosenzweig, Paradox of enrichment: Destabilization of exploitation ecosystems in ecological time, Science 171 (1971) 385–387.
[21] S. Ruan, D. Xiao, Global analysis in a predatorprey system with nonmonotonic functional response, SIAM J. Appl. Math. 61 (2001) 1445–1472.
[22] V. van G. A. K., L. Hemerik, M.P. Boer, B.W. Kooi, Heteroclinic orbits indicate overexploitation in predator–prey systems with a strong Allee effect, Math. Biosci. 209 (2007) 451–469.
[23] E. Venturino, A minimal model for ecoepidemics with group defense, J. Biol. Syst. 19 (2011) 763–785.
[24] E. Venturino, Ecoepidemiology: A more comprehensive view of population interactions, Math.Model. Nat. Phenom. 11 (2016) 49–90.
[25] E. Venturino, S. Petrovskii, Spatiotemporal behavior of a prey-predator system with a group defense for prey, Ecol. Complex. 14 (2013) 37–47.
[26] S. Wiggins, Introduction to Applied Nonlinear Dynamical Systems and Chaos, Texts in Applied Mathematics, Springer-Verlag, New York, 1990.